

Authors' response to Editor's comments

Journal : Ocean Sciences

Title of the paper: Impact of intraseasonal wind bursts on sea surface temperature variability in the far eastern Tropical Atlantic Ocean during boreal spring 2005 and 2006. Focus on the mid-May 2005 event.

Authors: Herbert Gaëlle, Bourlès Bernard

EC: Editor 's comments; **AC**: Authors' comments

EC: You have satisfactorily addressed the comments by the referee and your manuscript is now accepted for publication in Ocean Science. Before submitting the final version of your manuscript, please account for the last few technical issues listed below.

AC: We would like to thank the editor for his careful reading and valuable remarks. Additional small changes have been made following them as well as those offered by the reviewer, and we hope the revised manuscript will better suit the *Ocean Science*.

EC: Title, I suggest a minor modification (no abbreviations in the title; colon after the first part): Impact of intraseasonal wind bursts on sea surface temperature variability in the far eastern tropical Atlantic Ocean during boreal spring 2005 and 2006: Focus on the mid-May 2005 event

AC: The modification has been made.

EC: -L20, L21 anomalously strong

-L21 ... triggered the onset of coastal rainfall in the ... (the text was confusing; is this correct?)

-L22-23 I suggest: No similar atmospheric conditions were observed in May over the 1998-2008 period.

-L25 from the South Atlantic

-L147 "theta_s = 6 and theta_b = 0" Is this correct (format)?

-Data used: Is there any way to quantify the precision of the variables used?

You use data from other sources. Please check the fair data use policies and whether

you acknowledge the data originators adequately.

-L329, L339 1 March (format)

-L415 10 Feb 2006

-L553-554 please use consistent format

-L703 McPhaden

-L755, L758 Foltz et al., 2006 should be Foltz et al., 2003 according to the reference list

-L879 Journal: Science (typo), and change format.

-L1018 Deep-Sea Res.

AC: Thank you for pick up technical issues. The corrections have been made.

About “theta_s” and “theta-b”, it is the right format.

About the data used, we modified the text as follows for TMI data:

“The dataset is a merged product produced by Remote Sensing Systems and sponsored by the NASA Earth Sciences Program. The data are available at www.remss.com/missions/tmi.”
(l.170-171).

For sea surface height dataset:

“We also use for this study daily sea surface height (SSH) data, which are available for the period 1993–2012 and maintained by the organization for Archiving, Validation, and Interpretation of Satellite Oceanographic data with support from Cnes (AVISO; www.aviso.altimetry.fr/duacs). The sea surface height dataset is a merged product of observations from several satellite missions Ssalto/Duacs (Segment Sol multimissions d’ALTimétrie, d’Orbitographie et de localisation précise/Developing Use of Altimetry for Climate Studies) mapped onto a 0.25° Mercator projection grid.”

For ECMWF fields:

“In addition, surface pressure data were studied using ECMWF Atmospheric Reanalysis (ERA) for the 20th Century product (European Centre for Medium-Range Weather Forecasts, 2014). The four-hourly data are daily averaged and is available on <https://rda.ucar.edu> website. The product assimilates surface pressure and marine wind observations.”

About “Foltz et al., 2006” (l.755, 758), it is the correct citation. It refers to the reference noted in the reference list:

Foltz, G.R. and McPhaden, M.J.: Unusually warm sea surface temperatures in the tropical North Atlantic during 2005, Geophys. Res. Lett., 33: doi: 10.1029/2006GL027394. issn: 0094-8276, 2006.

Authors' response to reviewer's comments

Journal : Ocean Sciences

Title of the paper: Impact of intraseasonal wind bursts on sea surface temperature variability in the far eastern Tropical Atlantic Ocean during boreal spring 2005 and 2006. Focus on the mid-May 2005 event.

Authors: Herbert Gaëlle, Bourlès Bernard

RC: Reviewer's comments; **AC**: Authors' comments

RC: The authors have adequately addressed most of my concerns with the previous version of their manuscript. I recommend publication with some minor additional changes listed below.

AC: We would like to thank again the reviewer for the time and effort necessary to provide constructive remarks that contributed to improving the final version of our manuscript.

RC: Reviewer's comments; **AC**: Authors' comments

RC:

line 12: wind anomalies

line 165 and 167: removing FROM (not to)

line 256: Do you mean zonal?

line 346/347: z20 should most definitely not be the same as the mixed layer. I think what you mean to say is that mixed layer depth and thermocline depth do not necessarily show the same variability.

line 625, 628: RADSW needs to be explained (short wave radiation, I presume)

line 630: lowest (instead of weakest)

line 698/699: I find it very hard to follow that sentence.

line 729: as pronounced AS

line 733: I would suggest "importance" (instead of impact)

For Fig. 12, the caption is still not consistent with the labels of the subplots regarding the order of wind stress and radiation.

AC: Thanks for technical corrections. The modifications have been made.

About RADSW (line 625, 628 of the old version), the term is explained few lines above (line 618, 619 of the old version, line 620, 621 of the new version).

1 **Impact of intraseasonal wind bursts on sea surface temperature variability**
2 **in the far eastern Tropical Atlantic Ocean during boreal spring 2005 and**
3 **2006. Focus on the mid-May 2005 event.**

4 Gaëlle Herbert¹, Bernard Boulès¹

5 ¹:Institut de Recherche pour le Développement (IRD), Laboratoire d'Etudes Géophysiques et Océanographie Spatiale
6 (LEGOS), Brest, France.

7 *Correspondence to:* Gaëlle Herbert (gaelle.herbert@ird.fr)

8

9 **Abstract.** The impact of boreal spring intraseasonal wind bursts on sea surface temperature variability in the
10 eastern Tropical Atlantic Ocean in 2005 and 2006 is investigated using numerical simulation and observations.
11 We specially focus on the coastal region east of 5° E and between the equator and 7° S that has not been studied
12 in detail so far. For both years, the southerly **wind anomalies** induced cooling episodes through i) upwelling
13 processes; ii) vertical mixing due to vertical shear of the current; and for some particular events iii) a decrease
14 of incoming surface shortwave radiation. The strength of the cooling episodes was modulated by subsurface
15 conditions affected by the arrival of Kelvin waves from the west influencing the depth of the thermocline. Once
16 impinging the eastern boundary, the Kelvin waves excited westward-propagating Rossby waves which,
17 combined with the effect of enhanced westward surface currents, contributed to the westward extension of the
18 cold water. A particularly strong wind event occurred in mid-May 2005 and caused an anomalous strong cooling
19 off Cape-Lopez and in the whole eastern Tropical Atlantic Ocean. From the analysis of oceanic and atmospheric
20 conditions during this particular event, it appears that **anomalously** strong boreal spring wind strengthening
21 associated to anomalous strong Hadley cell activity prematurely triggered **the onset of coastal rainfall** in the
22 northern Gulf of Guinea, making it the earliest over 1998-2008 period. No similar atmospheric conditions were
23 observed in May over the 1998-2008 period. It is also found that the anomalous oceanic and atmospheric
24 conditions associated to the event exerted strong influence on rainfall off Northeast Brazil. This study highlights
25 the different processes through which the wind power from **the** South Atlantic is brought to the ocean in the
26 Gulf of Guinea and emphasizes the need to further document and monitor the South Atlantic region.

27

28 **1.Introduction**

29 The eastern equatorial Atlantic Ocean shows a pronounced seasonal cycle in sea surface temperature (SST)
30 (Wauthy, 1983; Mitchell and Wallace, 1992). One strong signature of the SST seasonal cycle in the eastern
31 equatorial Atlantic is the Atlantic cold tongue (ACT) (Zebiak, 1993) characterized by a fast drop of SST (up to
32 7° C) in boreal spring and summer slightly south of the equator and east of 20°W (Merle, 1980; Picaut, 1983).
33 During boreal summer, the southern boundary of this cooler temperature connects progressively with the austral
34 winter cooling of the Southern hemisphere SSTs. A number of observational (Merle, 1980; Foltz et al., 2003)
35 and modeling (Philander and Pacanowski, 1986; Yu et al., 2006; Peter et al., 2006) studies show that the

36 development of the ACT is driven by the seasonal increase of the Southern Hemisphere trade winds during late
37 boreal winter to early summer (Brandt et al., 2011) associated with the meridional displacement of the Inter-
38 Tropical Convergence Zone (ITCZ) (Picaut, 1983; Colin, 1989; Waliser and Gautier, 1993; Nobre and Shukla,
39 1996). The equatorial cooling is regulated by a coupling between thermocline shoaling, subsurface dynamics
40 (Yu et al., 2006; Peter et al., 2006; Wade et al., 2011; Jouanno et al., 2011) including turbulent mixing, vertical
41 advection and entrainment, as well as horizontal advection. The equatorial thermocline shoaling is the
42 consequence of local and remote wind forcing: the strengthening of easterly winds in the western equatorial
43 Atlantic remotely forces the seasonal upwelling in the eastern part of the basin via equatorial Kelvin waves
44 (Moore et al., 1978; Adamec and O'Brien, 1978; Busalacchi and Picaut, 1983; McCreary et al., 1984).

45 Besides the dominant seasonal cycle, the eastern tropical Atlantic is under the influence of meridional southerly
46 winds (Picaut, 1984) which fluctuate with a period close to 15 days (Krishnamurti, 1980; de Coëtlogon et al.,
47 2010; Jouanno et al., 2013). These intraseasonal wind fluctuations are therefore expected to be a major
48 contributor to the seasonal SST cooling and occur as an energy and momentum carrier from the South Atlantic
49 to the eastern equatorial Atlantic. A connection between the strength of the St. Helena Anticyclone and SST
50 anomalies in the southeastern tropical Atlantic has been described by Lübbecke et al. (2014). These authors
51 suggest that the St. Helena Anticyclone variability might be an important source of anomalous tropical Atlantic
52 wind power which affects SST in the eastern equatorial Atlantic via several mechanisms: zonal wind stress
53 changes in the western equatorial basin, wave adjustment, meridional advection of subsurface temperature
54 anomalies, intraseasonal wind stress variations, and possibly even other mechanisms. Through the in situ data
55 analysis of AMMA/EGEE cruises (Redelsperger et al., 2006; Bourlès et al., 2007) carried out in 2005 and 2006,
56 Marin et al. (2009) show that the SST seasonal cooling at the equator east of 10° W is not smooth but results
57 from the succession of short-duration cooling episodes generated by southeasterly wind bursts due to the
58 fluctuating St. Helena Anticyclone. In addition, according to Leduc-Leballeur et al. (2013), the sharp and
59 durable change in the atmospheric circulation in the northern Gulf of Guinea (durably strong southerlies north of
60 equator) takes place through an abrupt seasonal transition prepared by a succession of southerly wind bursts and
61 possibly triggered by a significantly stronger wind burst. The southerly wind bursts occurring in boreal spring in
62 the Gulf of Guinea thus would play an important role in driving precipitation pattern in the area through air-sea
63 interactions (de Coëtlogon et al., 2010; Nicholson and Dezfuli, 2013) and coupling between the ACT and the
64 West Africa Monsoon (WAM).

65 Improving our understanding of the impact of such wind bursts on SST variability at intraseasonal scale in the
66 eastern Tropical Atlantic is important through its link with the regional climate. However, while the ACT and
67 Angola-Benguela regions have been the object of many studies, the dynamics and SST variability of the coastal
68 eastern region is much less documented.

69 In this study, we therefore first focus our analysis off Cape-Lopez (defined from 0° N-7° S; 5° E-14° E and
70 hereafter called CLR for 'Cape-Lopez region', see Fig. 2) and aim to improve understanding of its seasonal SST
71 variability and the impact of intraseasonal winds on SST variability during boreal spring and summer. To this
72 end, we use regional high resolution model results as well as satellite SST data and sea surface height
73 observations. We first use model outputs from 1998 to 2008 to analyze the seasonal cycle in CLR and to

74 highlight its interannual variability, and then we specially focus on the years 2005 and 2006 to investigate the
75 SST response of intraseasonal wind forcing. These two particular years were largely investigated during the
76 African Monsoon Multidisciplinary Analyses (AMMA) experiment (Redelsperger et al., 2006). The year 2005
77 is characterized by the lowest SST values in the ACT during the past 3 decades (along with 1982), while 2006 is
78 considered as a normal year (Caniaux et al., 2011). Also, 2005 exhibits the earliest development of the ACT.
79 The study of SST variability at intraseasonal scale during these two years is thus interesting for better
80 understanding their observed differences in SST seasonal conditions. These two particular years have been also
81 chosen by Marin et al. (2009) to study the variability of the properties of the ACT. Their study concerned the
82 equatorial area west of 4° E, whereas we propose to focus in CLR, east of 5° E where coastal processes are
83 expected to be involved.

84 The question of the processes implied in the SST variability in the Cape-Lopez region was raised based on an
85 observation in satellite SST data of cold coastal waters during boreal spring independent from those observed
86 off shore in the cold tongue region around 10°W (see Fig. 2) which also raised the question of the link of such
87 cooling with the cold tongue development. Most studies on the CLR focused on the analysis of observational
88 data sets to examine the hydrology and its seasonal variation along the frontal (coastal) region of Congo (e.g.
89 Merle, 1972; Piton, 1988) or on the impact of Congo River on SST and mixed layer (e.g. Matera et al., 2012;
90 Denamiel et al., 2013; White and Toumi, 2014) but, to our knowledge, no detailed analysis of SST variability at
91 seasonal and intraseasonal time scales have been realized. A better understanding of ocean-atmosphere
92 interactions in this region is thus needed. Some previous studies related to the whole eastern Tropical Atlantic
93 (Gulf of Guinea) suggest that multiple processes could be at play in the CLR, coupling remote and local forcing.
94 For example, Giordani et al. (2013) show from regional model results that horizontal advection, entrainment,
95 and turbulent mixing significantly contribute to the heat budget east of 3°W because of the very thin mixed
96 layer. The upper layers of the north CLR might also be impacted by vertical mixing induced by the intense
97 current vertical shear between the South Equatorial Current, flowing westward at the surface, and the subsurface
98 eastward Equatorial Under-Current. In addition to local forcing, the area is also under the influence of the arrival
99 of equatorial Kelvin waves from West and their reflection, once reaching the African coast, poleward as
100 coastally trapped waves and westward as Rossby waves (Moore, 1968; McCreary, 1976; Moore and Philander,
101 1977). The principal source of the equatorial Kelvin waves has been usually related to the western equatorial
102 zonal wind changes during late boreal winter to early summer (e.g.; Philander, 1990). In order to better
103 understand the trigger mechanism of Kelvin waves generation which conditions the mixed layer properties in
104 the CLR, another purpose of this study is thus to identify the atmospheric conditions coinciding with the Kelvin
105 waves generation in the West of the basin during winter 2005 and 2006. In addition, some studies (such as
106 DeCoëtlogon et al., 2010) suggest that at short time scale (a few days), more than half of the cold SST anomaly
107 around the equatorial cooling could be explained by horizontal oceanic advection of upwelled cold coastal
108 waters controlled by the winds. Therefore, a better understanding of the SST variability in the CLR may also
109 help to better understand the SST variability in the equatorial region.

110 Several studies (e.g. Okumura and Xie, 2004; Caniaux et al., 2011; Nguyen et al., 2011; Thorncroft et al., 2011)
111 show evidence of a high correlation between the ACT and the WAM onset in the Sahelian region. Based on an

112 analysis of 27 years of data, Caniaux et al. (2011) identified the year 2005 as the year with the earliest WAM
113 onset date (around 19 May 2005 whereas they define the mean onset date on 23 June +/-8 days). According to
114 Marin et al. (2009), the time shift in the development of the ACT between 2005 and 2006 is related to a
115 particular wind burst event in mid-May 2005. This mid-May 2005 event therefore appears as exerting a strong
116 influence on the WAM. In a second part of the study, we thus focus on this particular wind event that preceded a
117 strong cold event in the far eastern Tropical Atlantic along with an early ACT development. We aim to describe
118 i) the atmospheric and oceanic conditions during this particular event; ii) to what extent it is involved in the
119 WAM system; and iii) which processes make it an exceptional event.

120 The remainder of the paper is organized as follows. In Sect. 2, the model and observational data used in this
121 study are described. The seasonal and interannual variability of SST, winds, currents, 20° C-isotherm depth and
122 sea surface heat flux in the CLR are analyzed in Sect. 3. The cooling episodes generated in response to southerly
123 wind bursts and the other forcing mechanisms implied in the CLR are investigated in details for the years 2005
124 and 2006 in Sect. 4. In Sect. 5, we focus our analysis on the unusual wind burst occurring in mid-May 2005.
125 Finally, the main results are summarized and discussed in Sect. 6.

126

127 **2. Model and data**

128 The numerical model used in this paper is the Regional Oceanic Modeling System (ROMS) (Shchepetkin and
129 McWilliams, 2005). The model configuration is the same as employed in Herbert et al. (2016), and the
130 following text is derived from there with minor modifications.

131 ROMS is a three-dimensional free surface, split-explicit ocean model which solves the Navier-Stokes primitive
132 equations following the Boussinesq and hydrostatic approximations. We used the ROMS version developed at
133 the Institut de Recherche pour le Développement (IRD) featuring a two-way nesting capability based on AGRIF
134 (Adaptative Grid Refinement In Fortran) (Debreu et al., 2012). The two-way capability allows interactions
135 between a large-scale (parent) configuration at lower resolution and a regional (child) configuration at high
136 resolution. The ROMSTOOLS package (Penven et al., 2008) is used for the design of the configuration. The
137 model configuration is built following the one performed by Djakouré et al. (2014) over the Tropical Atlantic.
138 The large scale domain extends from 60° W to 15.3° E and from 17° S to 8° N and the nested high resolution
139 zoom focuses between 17° S and 6.6° N and between 10° W and 14.1° E domain. This configuration allows for
140 equatorial Kelvin waves induced by trade wind variations in the western part of the basin to propagate into the
141 Gulf of Guinea and influence the coastal upwelling (Servain et al., 1982; Picaut, 1983). The horizontal grid
142 resolution is 1/5° (i.e. 22 km) for the parent grid and 1/15° (i.e. 7 km) for the child grid (see Herbert et al.
143 (2016), their Fig. 1). This allows an accurate resolution of the mesoscale dynamics since the first baroclinic
144 Rossby radius of deformation ranges from 150 to 230 km in the region (Chelton et al., 1998). The vertical
145 coordinate is discretized into 45 sigma levels with vertical S-coordinate surface and bottom stretching
146 parameters set respectively to $\theta_s = 6$ and $\theta_b = 0$, to keep a sufficient resolution near the surface
147 (Haidvogeland Beckmann, 1999). The vertical S-coordinate H_c parameter, which gives approximately the
148 transition depth between the horizontal surface levels and the bottom terrain following levels, is set to $H_c = 10$
149 m. The GEBCO1 (Global Earth Bathymetric Chart of the Oceans) is used for the topography (www.gebco.net).

150 The runoff forcing is provided from Dai and Trenberth's global monthly climatological run-off data set (Dai and
151 Trenberth, 2002). The rivers properties of salinity and temperature are prescribed as annual mean values. One
152 river (Amazon) is prescribed in the parent model while five rivers, that correspond to the major rivers present
153 around the Gulf of Guinea, are prescribed in the child model (Congo, Niger, Ogoou, Sanaga, Volta). At the
154 surface, the model is forced with the surface heat and freshwater fluxes as well as 6 hourly wind stress derived
155 from the Climate Forecast System Reanalysis (CFSR) (horizontal resolution of $\frac{1}{4}^{\circ} \times \frac{1}{4}^{\circ}$) (Saha et al., 2010). Our
156 model has three open boundaries (North, South, and West) forced by temperature and salinity fields from the
157 Simple Ocean Data Analyses (SODA) (horizontal resolution of $\frac{1}{2}^{\circ} \times \frac{1}{2}^{\circ}$) (Carton et al., 2000a, 2000b; Carton
158 and Giese, 2008). The simulation has been performed on IFREMER Caparmor super-computer and integrated
159 for 30 years from 1979 to 2008 with the outputs averaged every 2 days. A statistical equilibrium is reached after
160 ~10 years of spin-up. Model analyses are based on the 2-days averaged model outputs from year 1998 to year
161 2008. The model has already been validated successfully with a large set of measurements and climatological
162 data, and more detailed information about the model validations can be found in Herbert et al. (2016).
163 Note that throughout the whole text and figure captions, the term "intraseasonal variations" is used to designate
164 the field obtained after removing the 30 days low-pass filtered field from the total field of the given year, while
165 "intraseasonal anomaly" refers to the field obtained after removing the 30 days low-pass filtered field averaged
166 over 1998-2008 from the total field of the given year.

167

168 For SST observations, we use data obtained from measurements made by the Tropical Rainfall Measuring
169 Mission microwave imager (TMI). The dataset is a merged product produced by Remote Sensing Systems and
170 sponsored by the NASA Earth Sciences Program. The data are available at www.remss.com/missions/tmi. The
171 SST data have a spatial resolution of $\frac{1}{4}^{\circ}$ and for the present study the 10 years' time series, from 1 January 1998
172 to 31 December 2008, obtained as 3-daily field. The important feature of the microwave retrievals is that it can
173 give accurate SST measurements under clouds (Wentz et al., 2000). However, the major limitation to the
174 microwave TMI observations is land contamination which results in biases of the order of 0.6°K within about
175 100 km from the coast (Gentemann et al., 2010). Thus, in the Optimal Interpolation TMI product the offshore
176 zone with no data extends at approximately 100 km from the coast. This limits to some degree the analysis of
177 near-coastal regions, in particular those dominated by coastal upwelling dynamics.

178 We also use for this study daily sea surface height (SSH) data, which are available for the period 1993–2012 and
179 maintained by the organization for Archiving, Validation, and Interpretation of Satellite Oceanographic data
180 with support from CNES (AVISO; www.aviso.altimetry.fr/duacs). The sea surface height dataset is a merged
181 product of observations from several satellite missions Ssalto/Duacs (Segment Sol multimissions d'ALTimétrie,
182 d'Orbitographie et de localisation précise/Developing Use of Altimetry for Climate Studies) mapped onto a
183 0.25° Mercator projection grid. All standard corrections have been made to account for atmospheric (wet
184 troposphere, dry troposphere and ionosphere delays) and oceanographic (electromagnetic bias, ocean, load, solid
185 Earth and pole tides) effects. The mean sea surface topography for the period 1993–2012 was removed from the
186 SSH to produce sea surface height anomalies.

187 In addition, surface pressure data were studied using ECMWF Atmospheric Reanalysis (ERA) for the 20th
188 Century product (European Centre for Medium-Range Weather Forecasts, 2014). The four-hourly data are daily

189 averaged and is available on <https://rda.ucar.edu> website. The product assimilates surface pressure and marine
190 wind observations.

191

192 **3. Seasonal variability of surface conditions in CLR**

193 The purpose of this section is to describe the seasonal atmospheric and ocean surface conditions in the CLR.

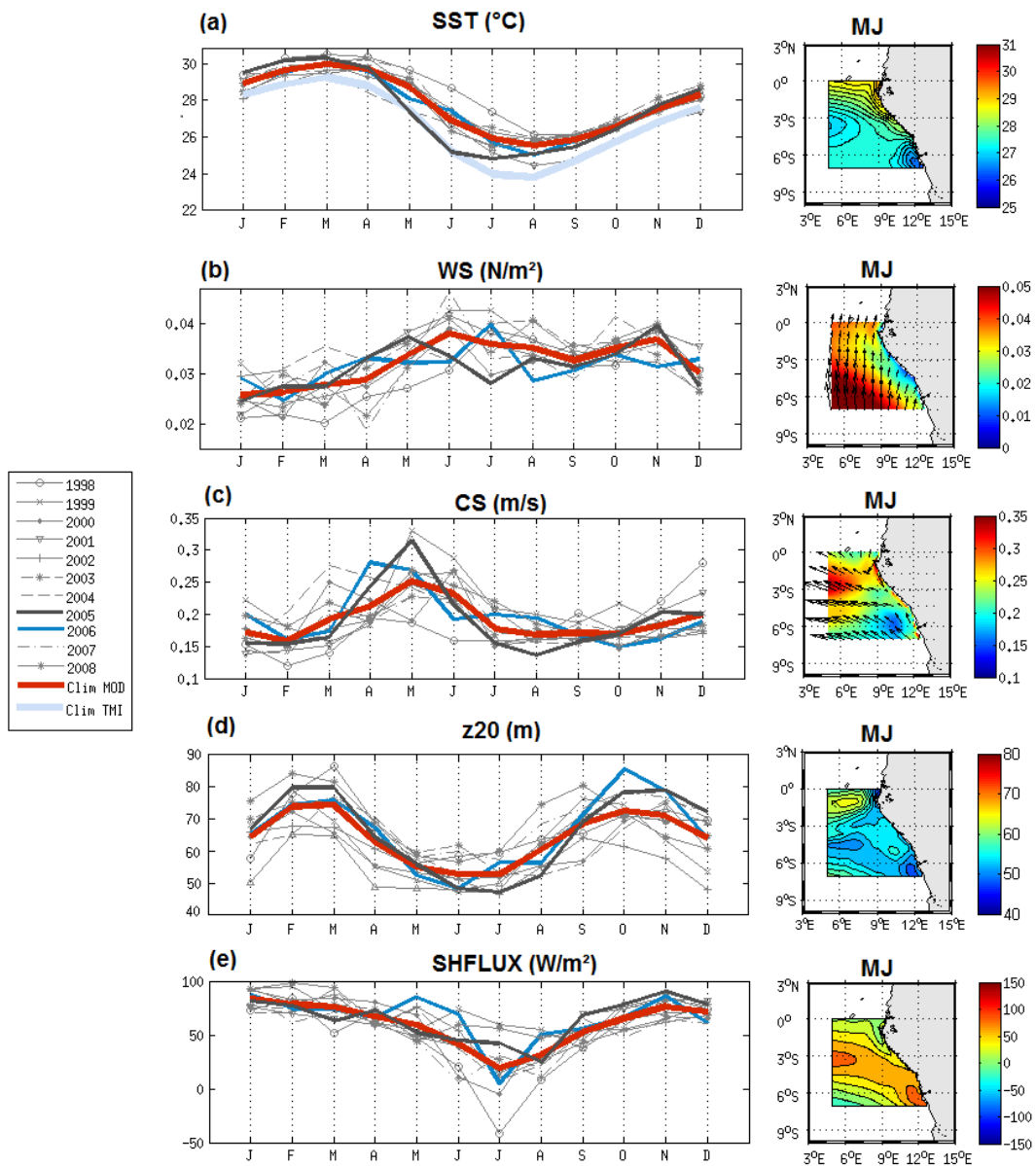
194 The seasonal variability of SST, surface winds stress, horizontal current intensity, depth of 20° C-isotherm
195 (hereafter referred to as z20), and the surface net heat flux from monthly averaged model outputs in the CLR for
196 each year from 1998 to 2008 and averaged over the period are shown in Fig. 1. The reliability of the model is
197 also provided by comparing the simulated and the corresponding TMI SST climatological seasonal cycle in the
198 CLR (Fig. 1a). The SST variations display an annual cycle with highest temperature at the end of boreal winter
199 – beginning of boreal spring (warm season), when the ITCZ reaches its southernmost position and the trade
200 winds are weakest, and minimum values in boreal summer (cold season), when the trades intensify. The most
201 salient features of the atmospheric and hydrographic fields during May-June are also illustrated in Fig. 1 by
202 May-June averaged maps. Despite a warm bias (~1°C) compared to satellite observations, the model reproduces
203 the satellite pattern well. While this warm bias in the eastern tropical Atlantic is well known in coupled climate
204 models (e.g. Zeng et al., 1996; Davey et al., 2002; Deser et al., 2006; Chang et al., 2007; Richter and Xie, 2008),
205 results from Large and Danabasoglu (2006) suggest indeed that a warm SST bias may also be present along the
206 Atlantic coast of southern Africa in forced ocean-only simulation. The SST May-June average map indicates
207 that the boreal summer SST minimum is related to intensified cool SST around 6°S, in the Congo mouth region.
208 In this region, the coast is oriented parallel to the trade flow which reinforces in boreal summer, thus favorable
209 to coastal upwelling processes. The mean alongshore wind stress during May-June reveals in fact that upwelling
210 conditions are observed over most of the CLR. The coastal upwelling could also interact with the coastal Kelvin
211 wave propagation (e.g. Ostrowski et al., 2009) highlighted by minimum z20 values in Fig. 1d.

212 Wind stress magnitude exhibits a semi-annual variability with a second maximum in October–December and a
213 weakening during July-September season (Fig. 1b). The strengthening of winds in boreal spring is associated
214 with a strengthening of mean current speed, particularly off Cape-Lopez between 2° S to 4° S and west of 8° E
215 in May-June (Fig. 1c). The orientation of surface current is mostly westward for the May-June season, while it is
216 northward from October to January (not shown). This general picture of surface circulation is consistent with
217 observations (Merle, 1972; Piton, 1988; Rouault et al., 2009).

218 The region is also characterized by a shallow thermocline which depicts a strong semi-annual cycle (Fig. 1d).
219 The evolution of z20 reveals a shoaling of the thermocline during May-July and a deepening up to October-
220 November when it exhibits a maximum depth, in agreement with previous studies such as the one realized by
221 Schouten et al. (2005) who find a similar seasonal cycle from SSH altimetric data.

222 The surface net heat flux exhibits a maximum in boreal winter and a minimum in July (Fig. 1e), following the
223 seasonal cycle of solar shortwave radiations. As visible on the May-June average map, greater heating is found
224 over cool waters, due to weaker heat loss via latent heat flux in these areas.

225 The seasonal cycle is modulated by strong year-to-year variations. The mean SST in the CLR in 2005 cools as
 226 early as March from TMI data and April from the model data. SST reaches lower values than the climatologic
 227 ones, as observed by Marin et al. (2009) and Caniaux et al. (2011) west of 4° E. This 2005 cold anomaly is
 228 associated with positive wind speed and surface current speed anomaly in April-May (Fig. 1b&c) as well as
 229 shallower-than-average thermocline depth. In 2006, SST variations are very close to the climatologic ones.
 230
 231 Thus, the April-June season in the CLR appears as a transitional period characterized by strong seasonal
 232 evolution, primarily governed by the local winds which generate coastal upwelling in Congo mouth region and
 233 modulated by the variation of thermocline depth.



235 **Figure 1:** Monthly average of the (a) sea surface temperature ($^{\circ}\text{C}$); (b) wind stress direction (vectors) and
236 magnitude (color field) (N.m^{-2}); (c) horizontal surface current direction (vectors) and speed (color field) (m.s^{-1});
237 (d) 20° C-isotherm depth (m); and (e) surface heat flux (W.m^{-2} ; positive values indicate downward flux) from
238 January to December from 1998 to 2008 and for the climatology (averaged over 1998-2008) simulated by the
239 model (red curve) and from the observations : monthly average TMI 3-daily SST data (light blue curve in (a));
240 averaged over 5° E- 14° E and 7° S- 0° S. Right panel: maps of each variable over May-June..

241

242 **4. Analysis of cooling episodes in the CLR in 2005 and 2006**

243 In this section, we examine the impact of intraseasonal wind bursts on SST in the CLR during the particular
244 years 2005 and 2006 (Marin et al., 2009; Caniaux et al., 2011). We propose here to analyze in details the SST
245 conditions in CLR, east of 5° E, for both years.

246

247

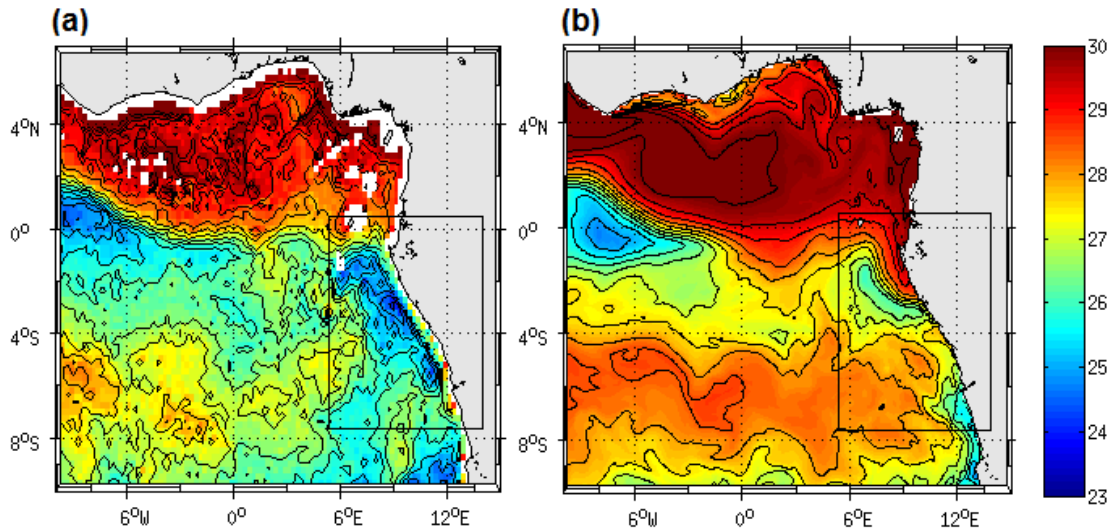
248 **4.1 SST variations**

249 In order to delineate the sequence of cooling episodes, we analyze the SST variations from 2-days averaged
250 model outputs in 2005 and 2006 over the CLR, i.e. between 5° E and 12° E. Both the SST (Fig. 3a & c) and
251 intraseasonal variations of SST (Fig. 4a & f) are shown. The cooling episodes occurred east of 5° E from April
252 to September. In 2005, the intraseasonal cooling episodes took place on 8-12 May, 16-22 May, 30 May-June 6,
253 and 12-16 June, whereas in 2006, they took place on 20-30 April, 14-24 May, 14-20 & 26-30 June. The
254 temperature drop for the two years ranged between -0.2°C to -2°C . The cooling episodes concerned especially
255 the southern equatorial region (around $\sim 3-4^{\circ}$ S), except for the strongest events where they reached more
256 northern equatorial regions, especially for the mid-May and late-May 2005 events. These latter were associated
257 with an intense SST front between the cold water south of the equator and the warmer water north of the
258 equator, as visible on SST map for 12 May 2005 presented in Fig. 2. We can see cold waters extending along
259 the eastern coast and in ACT region west of 5° W. In the model, cold waters are deflected offshore off Cape-
260 Lopez, due to recursive bias in warm water intrusion toward the south.

261 Besides, model SST fields (Fig. 3a) indicate that the SST minimum ($\sim 24^{\circ}$ C) in 2005 was reached in July, i.e.
262 one month earlier than in 2006, as also noticed in seasonal variations of SST averaged in the region (Fig. 1a).
263 These results illustrate the important role of the succession of quick and intense cooling episodes in the
264 establishment of persistent cold anomalies in the CLR, as highlighted by Marin et al. (2009) in the equatorial
265 region.

266

267



268

269 **Figure 2:** Map of the sea surface temperature ($^{\circ}$ C) on 12 May 2005 from 3-days average TMI data (a) and from
 270 the 2-days average model output (b). Note that for the model it corresponds to 11-12 May average whereas for
 271 TMI data it is 10-11-12 May average. The black square indicates the Cape-Lopez region (called ‘CLR’).

272

273 4.2 Forcing mechanisms

274 4.2.1. Local forcing

275 To examine the local forcing mechanisms responsible for the observed cooling episodes in CLR, the
 276 intraseasonal variations of wind stress magnitude are examined and compared in 2005 and 2006 (Fig. 4b & 4g).
 277 In 2005, successive periods of 6-16 days wind intensification occurred from late-March to late-June. The main
 278 cooling episodes described above are associated with positive intraseasonal wind stress speed occurring on 6-8,
 279 14-18 & 26-30 May, and 10-14 & 28 June-2 July with a maximum for the 14-18 May event peaking on 16 May
 280 (at $\sim 0.025 \text{ N.m}^{-2}$). Another period of wind intensification is evident in late March – early April but it did not
 281 generate significant cooling despite comparable or even higher wind intensity than following wind events. In
 282 2006, periods of wind intensification extended from mid-March to July. The main wind events in boreal spring
 283 occurred in 2-4 & 16-24 April, 6-8 & 14-20 May, 14-16 & 24-26 June with maximum intraseasonal wind stress
 284 magnitude in 16-24 April (0.019 N.m^{-2}) and 24-26 June (0.022 N.m^{-2}). Also, the wind event in late April 2006
 285 did not generate a surface cooling as strong as the mid-May 2006 one, despite higher wind stress magnitude. To
 286 depict the subsurface conditions during cooling episodes in the CLR for both years, the 20° C-isotherm depths
 287 averaged from 5° E to 12° E are presented in Fig. 3b & 3d. They indicate strong correlation with SST variations
 288 on intraseasonal time scale with minimum depths ($< 35 \text{ m}$) observed during the mid-May 2005 and end-May
 289 event. In early April 2005 and before the late-April 2006, the thermocline was deeper, that can explain why
 290 wind intensification did not generate a surface cooling at these times. Indeed, at the time of the strong 16-24
 291 April 2006 wind event, the z_{20} values was higher south of the equator than during the 14-16 May 2005 event,
 292 making the SST less reactive to comparable wind intensification. The same feature is observed in early May
 293 2006, when the higher z_{20} values indicate deeper thermocline south of the equator around $3\text{-}4^{\circ}$ S than a few

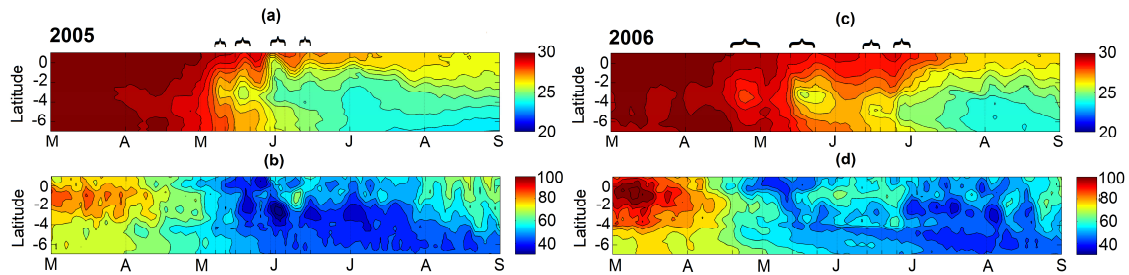
294 days later. Besides, the thermocline appeared shallower south of the equator in 2005 than in 2006, in agreement
295 with the difference of the cooling intensity observed between the two years.

296 The Ekman pumping velocity w_e averaged over the CLR for 2005 and 2006 is shown in Fig. 4d & 4i
297 respectively. The dates of intraseasonal upward velocities are quite well correlated with the dates of
298 intraseasonal wind events (with correlation coefficient equal to 0.55 for 2005 and 0.41 for 2006), maximum
299 being during the early-April, mid-May and end-May 2005 events and during .late April, mid-June and end-June
300 2006. However, for comparable wind intensification, the boreal spring and summer wind events were not
301 associated with comparable intensity of Ekman pumping velocity.

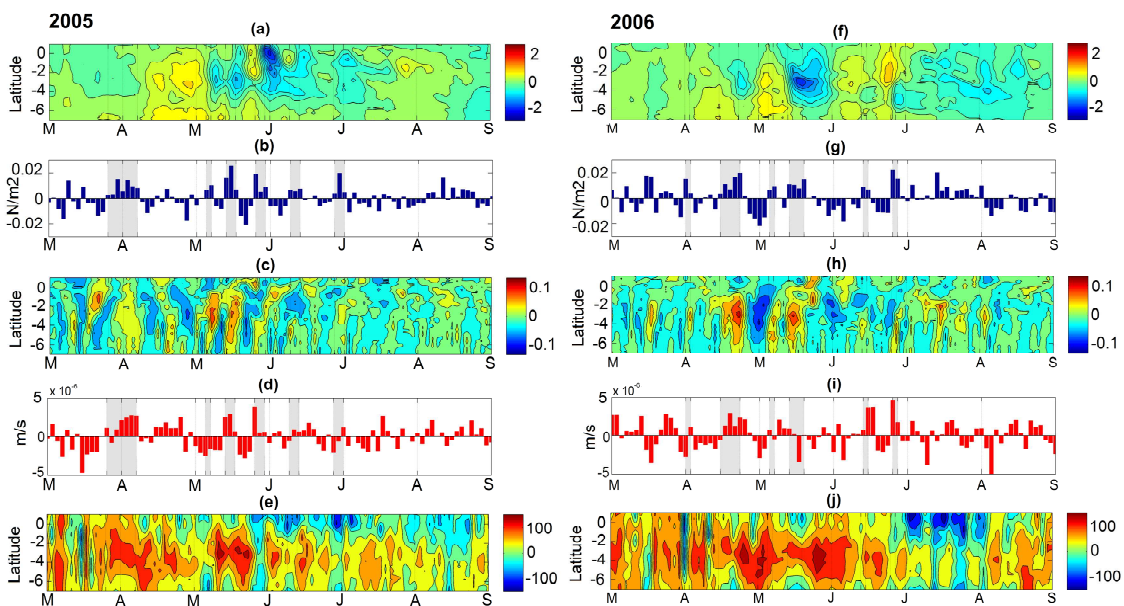
302 Another process that may contribute to the cooling in the upper layer is the vertical mixing due to intense
303 vertical shear of the current. The maximum of the vertical shear magnitude fields in the CLR, averaged between
304 5° and 12° E for 2005 and 2006 (Fig. 4c & 4h), exhibited intensification south of the equator, centered around 3-
305 4° S. Weaker intensification also occurred occasionally at the equator (located around 80 m depth between the
306 westward surface South Equatorial Current – SEC – and the eastward subsurface Equatorial Under- Current).
307 Around 3-4°S, the vertical shear was driven by the SEC, reinforced by prevailing southerly winds events
308 through Ekman transport. It thus occurred at the date of wind events previously identified for 2005 and 2006,
309 with stronger vertical shear occurring in early May 2005 and late April 2006. The intensity of the maximum of
310 vertical shear magnitude during the events was quite similar between 2005 and 2006. The main difference lied
311 in their meridional extent, related to the meridional extent of the strengthened southerly winds which reached
312 equatorial region during the May 2005 events (not shown). We can also notice that for comparable wind
313 intensification, the boreal spring and summer wind events were not associated with comparable intensity of
314 vertical shear. The meridional wind component favorable to westward Ekman transport was actually stronger
315 during April and May events than during summer ones (not shown).

316 The heat content within the mixed layer is also impacted by the sea surface heat fluxes.
317 The net heat fluxes averaged between 5° E and 12° E are shown in Fig. 4e & 4j for 2005 and 2006 respectively.
318 They indicate a net heating (~ 50 - 100 W.m^{-2}) over the 2° S - 5° S latitude band, where the SST cooling was
319 strongest, suggesting other mechanisms involved. However, we notice some particular events during which the
320 net heat flux was negative over most of the region. A strong net cooling (-30 W.m^{-2}) occurred during the 26-28
321 May 2005 event. It was mainly due to a sudden decrease of incoming surface short wave radiation (drop of
322 about 80 W.m^{-2} in the CLR between 22 and 28 May; not shown) suggesting increased cloud cover. Another
323 strong net cooling occurred on 2 April 2006 with a mean value in the CLR reaching -95 W.m^{-2} . It is more sudden
324 than the end-May 2005's one, and was almost exclusively restricted to the CLR region with values reaching
325 locally -185 W.m^{-2} (not shown). For both events, the net cooling did not concern the equatorial region west of
326 0° W.

327



328
 329 **Figure 3:** (a & c) Latitude-time diagram of the sea surface temperature (°C) averaged between 5°E and 12°E; (b
 330 & d) Latitude-time diagram of the 20° C-isotherm depth (m) averaged between 5° E and 12° E; from 1 March
 331 to 31 August 2005 (left panels) and 2006 (right panels). The cooling episodes are indicated by the black
 332 brackets.



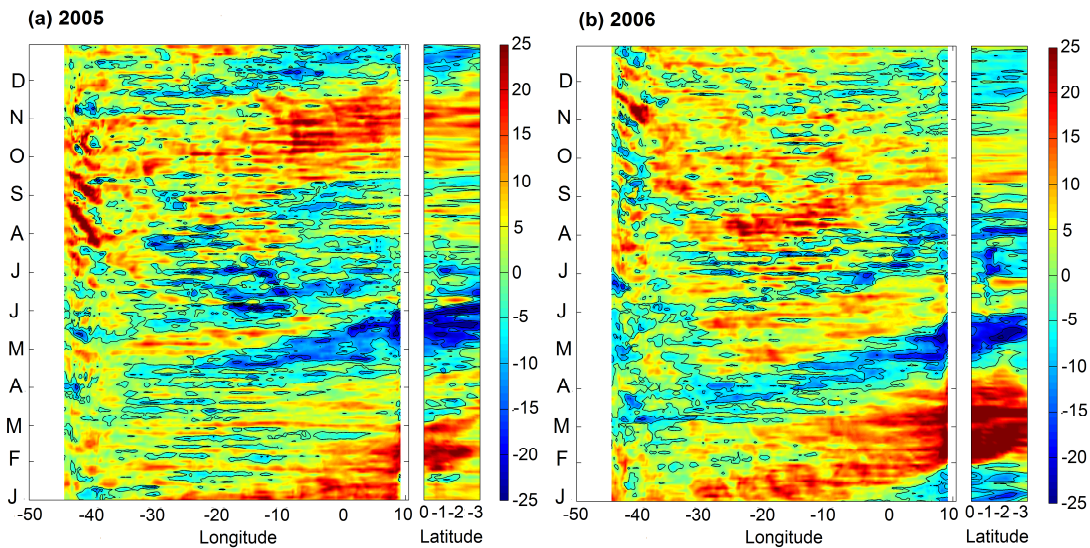
333
 334 **Figure 4:** (a & f) Time-latitude diagram, from 7° S to 1° N, of the intraseasonal variations of sea surface
 335 temperature (in ° C) averaged between 5° E and 12° E; (b & g) Time evolution of the intraseasonal variations of
 336 wind stress amplitude ($N.m^{-2}$) averaged between 5° E and 12° E and between 3° S and 0° S; (c & h) Latitude-
 337 time diagram of the intraseasonal variations of the maximum of the current vertical shear magnitude ($m.s^{-1}$)
 338 averaged between 5° E and 12°E; (d & i) Longitude-time diagram of the intraseasonal variations of Ekman
 339 Pumping ($m.s^{-1}$) averaged over the CLR. Ekman pumping values >0 indicate upwelling; (e & j) Latitude-time
 340 diagram of the net heat flux ($W.m^{-2}$) averaged between 5° E and 12° E; from 1st March to 31 August 2005 (left
 341 panels) and 2006 (right panels). For details about calculations of intraseasonal variations, see Sect. 2. The
 342 intraseasonal southerly wind events are indicated by the shaded areas. Note that the cooling episodes occur few
 343 days after the southerly wind events.

344 4.2.2. Remote forcing

345 a. Highlighting of Kelvin wave propagation

346 As previously shown, the time of occurrence of the cold events in the CLR coincides with shallow thermocline
 347 **which contributes to making the mixed layer temperature more reactive to surface forcing (note that z20 does**
 348 **not necessarily show the same variability as the mixed layer depth).** Indeed, because of its proximity to the
 349 equator, the thermocline in the CLR is affected by the arrival of equatorial waves, initiated in the western part of
 350 the basin. Pairs of alternate downwelling and upwelling Kelvin waves occur usually in February-March, July-
 351 September and October-November. Upon impingement with the eastern boundary, the incoming equatorial
 352 Kelvin wave excites westward-propagating Rossby waves and poleward-propagating coastal Kelvin waves
 353 (Moore, 1968; Moore and Philander, 1977; Illig et al., 2004; Schouten et al., 2005; Polo et al., 2008). The 20°
 354 C-isotherm depth anomalies along the equator and along 9°E are presented in Fig. 5 and clearly evidence large
 355 negative anomalies indicating shallower-than-average thermocline, propagating eastward along the equator and
 356 then southeastward for both years. The eastward propagation of Kelvin wave along the equator and
 357 southeastward along the coast is also well visible in the basin-wide SSH anomalies (Fig. 6) with a phase
 358 velocity of about 1.1-1.3m.s⁻¹, which fits well in the range between the second and third baroclinic equatorial
 359 Kelvin wave modes. In 2005, negative SSH and z20 anomalies occurred in the West in early March- early April
 360 and in mid-May, whereas they occurred around late-February – mid-March and early May and June in 2006.
 361 The first Kelvin wave thus reached the CLR slightly earlier in 2006 than 2005, at the beginning of May. In
 362 addition, the two upwelling Kelvin waves followed each other more closely in 2005 than in 2006.

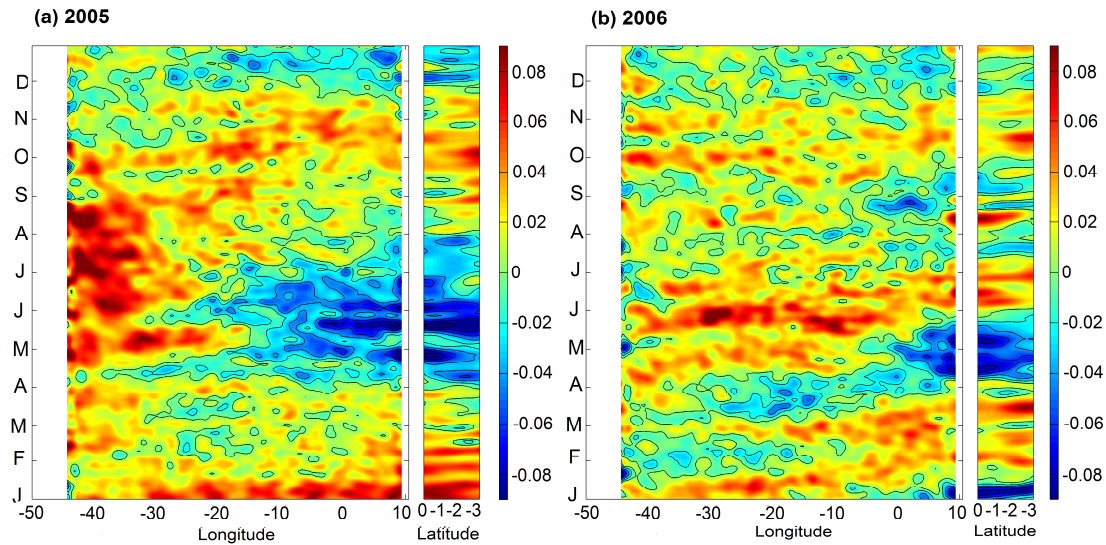
363 Thus, the intensity of the cold events observed in boreal spring and summer 2005 and 2006 resulted from both
 364 the basin preconditioning by remotely forced shoaling of the thermocline, local mixing and upwelling processes
 365 in response to strong southerly local winds, as well as heat flux variations. In 2005, stronger wind intensification
 366 and favorably preconditioned oceanic subsurface conditions, made the coupling between surface and subsurface
 367 ocean processes more efficient than in 2006, resulting in stronger cooling.
 368



369

370 **Figure 5:** Time evolution of the intraseasonal anomaly of 20° C-isotherm depth (m) along the equator (between
 371 54° W and 12° E) and along 9° E (between the equator and 3° S) for 2005 (left) and 2006 (right). Negative

372 values indicate a 20°C isotherm depth closer to the surface. For details about calculations of the anomalies, see
 373 Sect. 2.
 374



375

376 **Figure 6:** Time evolution of the sea level anomaly (m) along the equator (between 54° W and 12° E) and along
 377 9° E (between the equator and 3° S) for 2005 (left), and 2006 (right) from AVISO data.

378

379

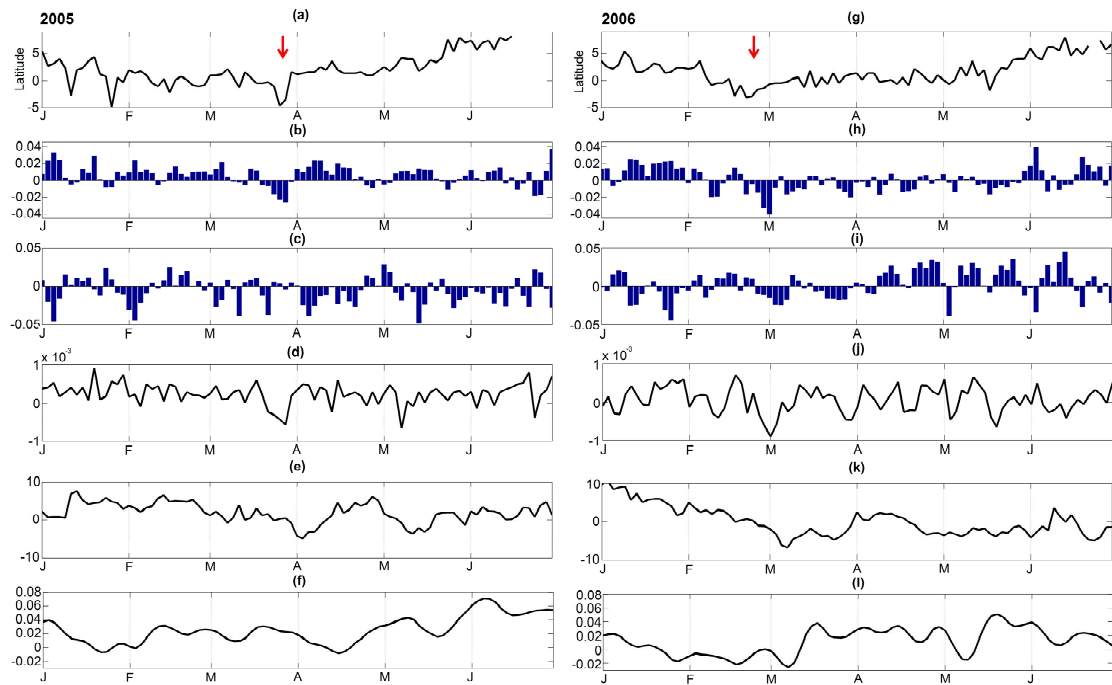
380 **b. Kelvin wave generation and coinciding atmospheric conditions in the West**

381 In order to identify the wind activity which accompanies the generation of Kelvin upwelling waves in winter
 382 2005 and 2006 in the western part of the basin, we analyze the position of the ITCZ (averaged over 50° W-35°
 383 W) identified as the latitude where the meridional wind stress goes to zero (Fig. 7a & g). The intraseasonal
 384 anomaly of the zonal and meridional components of the wind stress (Fig. 7b-c & 7h-i), the intraseasonal
 385 anomaly of wind stress curl (Fig. 7d & j), as well as the intraseasonal anomaly of the z20 and SSH (Fig. 7e-f &
 386 k-l), averaged in the equatorial band (over 1° S and 1° N), are also presented. Many authors suggest that the
 387 source of the equatorial Kelvin wave is mainly related to a sudden change of the western equatorial zonal wind
 388 (e.g. Picaut, 1983; Philander, 1990): a symmetric westerly (easterly) wind burst along the equator will generate
 389 Ekman convergence (divergence) and thus force downwelling (upwelling) anomalies which then propagate
 390 eastward as a Kelvin wave (Battisti, 1988; Giese and Harrison, 1990). In 2005, shallower-than-average
 391 thermocline, evidenced by negative z20 and SSH anomalies, occurred in the end of March-beginning of April in
 392 the west part of the basin (Fig. 7e & f). The intraseasonal anomalies of meridional and zonal wind stress indicate
 393 that the maximum of thermocline slope anomaly was associated with a strengthening of northeast trades
 394 followed by a strengthening of southeast trades from either side on the equator. At the equator, we notice indeed
 395 a sudden reversing of meridional winds which turned southward on 27-28 March 2005 related to an abrupt
 396 southward displacement of the ITCZ which was then found south of the equator in the west part of the basin

397 (Fig. 7a & b). The ITCZ returned its initial position four days later followed by a strengthening of easterlies
398 which persisted for ~20 days (Fig. 7c). Climatologically, the latitudinal position of the ITCZ varies from a
399 minimum close to the equator in boreal spring (March-May) in the west to a maximum extension of 10°N –
400 15°N in late boreal summer (August) in the east. Positive (negative) wind stress curl is found north (south) of the
401 ITCZ. When the ITCZ is north of the equator, it induces upward (downward) Ekman pumping to the north
402 (south) of the ITCZ. Thus, the southward shift of the ITCZ on 27-28 March 2005 accompanied with strong
403 northerlies led to negative anomaly of wind stress curl south of the equator resulting in upward Ekman pumping.
404 Results show indeed a strong negative anomaly on 22-26 March 2005 associated with the southward shift of the
405 ITCZ just before the upwelling signal, initiated on 28 March. These changes contributed to a rise in the oceanic
406 thermocline with a time lag of some days (Fig. 7e & f). The upwelling signal might then be reinforced by the
407 symmetric easterly wind which concerned a large part of the western basin. Besides, we identify in Fig. 7d
408 another peak of negative wind stress curl anomaly on 6-8 May 2005, more sudden than the previous winter one.
409 It was associated with negative z20 SSH anomalies indicator of a thermocline rise initiated on 6 May 2005 in
410 the west of the basin and which propagated eastward along the equator. The zonal wind stress anomalies (Fig.
411 7c) also indicate an easterly wind strengthening initiated in the beginning of May, which a maximum on 8-10
412 May, just after the minimum of wind stress curl.

413 In 2006, the upwelling Kelvin wave is identified in the first half of March in the west part of the basin (Fig. 7k
414 & l). The coinciding atmospheric conditions were slightly different than the ones identified in 2005. In winter,
415 the position of the ITCZ had a more southern position in 2006 than in 2005. It crossed the equator during a
416 longer period (about 10 days from ~ 10 Feb. 2006), reaching minimum latitude on 22-24 February. This location
417 south of the equator induced a negative wind stress curl anomaly (Fig. 7j). As in 2005, the reversion of the
418 meridional wind at the equator was followed by a strengthening of westward component of the wind stress few
419 days after, which lasted for about ten days (Fig. 7i); however, it was of a lesser magnitude compared to 2005
420 and only concerned the westernmost part of the basin. In addition, the negative zonal wind anomaly concerned
421 mainly the northeasterlies rather than the southeasterlies, leading to an anti-symmetric meridional wind pattern as
422 well as symmetric zonal wind pattern on either side on the equator (not shown). These wind patterns were
423 expected to generate Ekman divergence at the Equator and thus to reinforce the observed upwelling anomalies.

424
425 Thus, for both years, upwelling Kelvin waves were generated in the west while easterly winds were
426 strengthened from either side of the equator after the ITCZ reached its southernmost location. This latter was
427 observed one month earlier in 2006 than in 2005, and was associated with a negative wind stress curl anomaly.
428 In winter 2005, the ITCZ was found south of the equator after a very sudden southward shift and was followed
429 by strong easterlies during ~20 days, while in winter 2006, the ITCZ was found closer to the equator less
430 sharply and during a longer period, followed by weaker easterlies compared to 2005. These results highlight
431 another way in which intraseasonal wind events may impact the SST variability in the eastern part of the basin,
432 through the generation of Kelvin wave in the West which shoals the thermocline in the East a few weeks later.



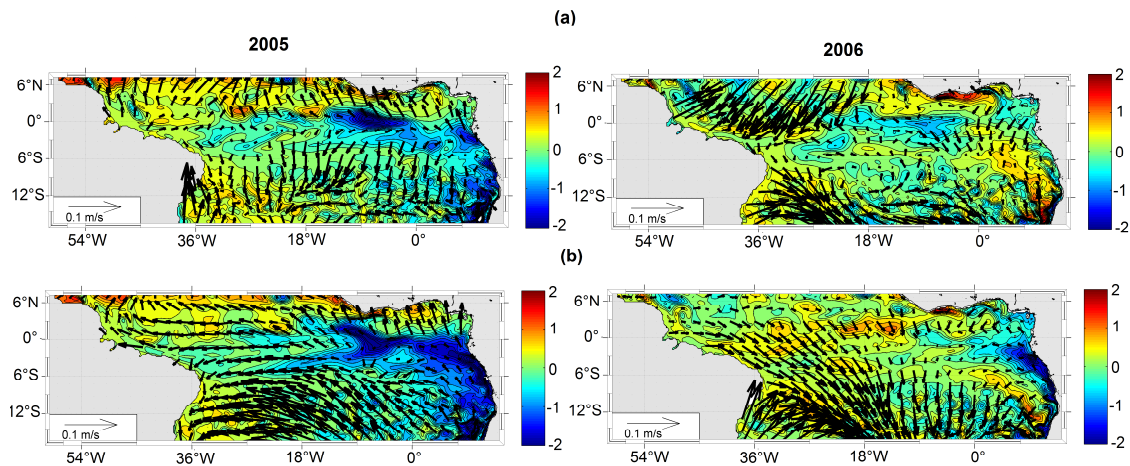
433

434 Figure 7: Time evolution, from 2-days averaged model outputs over Jan-June2005 (left) and Jan-June 2006
 435 (right); of (a & g) the position (in latitude, between 5° S and 10° N) where the meridional wind stress value
 436 equal zero (indicator of the position of the ITCZ); (b & h) the intraseasonal anomaly of the meridional wind
 437 stress ($N.m^{-2}$) averaged between 50° W and 35° W and between 1° S and 1° N; (c & i) same as (b & h) but for
 438 intraseasonal anomaly of zonal wind stress ($N.m^{-2}$); (d & j) the intraseasonal anomaly of the wind stress curl
 439 ($N.m^{-2}$); (e & k) the intraseasonal anomaly of the 20° C isotherm depth (m); negative values indicate that the
 440 20°C isotherm depth is closer to the surface; (f & l) the intraseasonal anomaly of the sea level (m). The red
 441 arrow in (a & g) indicates the southward shift of the ITCZ before the generation of the Kevin wave (see text).
 442 For details about the calculations of anomalies, see Sect. 2.

443

444 4.3. Westward extension of the CLR cooling

445 In the east, the cooling generated by southerly wind bursts in the CLR then progressively extended westward to
 446 connect with the southern boundary of the equatorial ACT. This phenomenon was more obvious in 2005 when
 447 the cooling which first concerned the coastal area extended further offshore a few days after the two strong
 448 events occurring in the second half of May. To evidence the effect of these events on SST, maps of
 449 intraseasonal SST anomaly and intraseasonal wind stress anomaly averaged from 1 to 12 May (before the strong
 450 2005 events; Fig. 8a) and from 14 to 31 May (during and after the strong 2005 events; Fig. 8b) are presented in
 451 Fig. 8. The same calculations have been made for 2006 for comparison. The results illustrate an enhancement
 452 after 10 May of the cooling in the east associated with southerly wind intensification and an extension of the
 453 cooling especially south of the equator up to 20°W.



454

455 **Figure 8:** (a) intraseasonal anomaly of sea surface temperature ($^{\circ}$ C; color) superimposed with intraseasonal
 456 anomaly of wind stress intensity (arrows) averaged over 1-12 May 2005 (up panel) and over 14-30May
 457 panel); (b) same but for 2006. For details about the calculations of the anomalies, see Sect.2.

458 To better understand the oceanic processes implied in this cooling extension, we compared the SST, z20, SLA
 459 and zonal velocities along 3° S from March to September 2005 (Fig. 9 a-d) and 2006 (Fig. 9 e-h). In 2005, the
 460 cooling westward extension was associated with a westward propagation of a shallower thermocline and
 461 negative SLA from the African coast up to 5° - 10° W combined with enhanced surface westward current
 462 fluctuations at the dates of the successive events from April-June. The fluctuations of the westward surface
 463 current occurring off Gabon with periods of \sim 8-10 days were related to the strengthening of southerly winds
 464 during the wind bursts at the same periods (Fig. 4b & g). The surface current in this area is part of the westward
 465 SEC which is known to intensify during the cold season (Okumura and Xie, 2006). Our study implies shorter
 466 time scales than seasonal scale but the intensification of the SEC during wind bursts through Ekman transport
 467 processes might contribute to the westward extension of the cooling by advection of cold eastern upwelled
 468 water. This is in agreement with DeCoëtlogon et al. (2010) who found from model results that at short time
 469 scale (a few days), more than half of the cold SST anomaly around the equatorial cooling could be explained by
 470 horizontal oceanic advection controlled by the wind with a lag of a few days. In addition, minimum z20 and
 471 SLA values propagating westward at 3° S (Fig. 9b & c), initiated from the coast with a propagating speed of
 472 around 10 cm.s^{-1} , which is very close to the phase speed of Rossby waves. Indeed, the generation of the
 473 westward waves at the coast coincided with the arrival of Kelvin waves (see Fig. 5a) suggesting the possibility
 474 of Kelvin wave's reflection processes into symmetrical westward propagating Rossby waves. A westward
 475 propagation of z20 and SLA minimums, although less obvious, was presently also identified at 3° N (not
 476 shown).

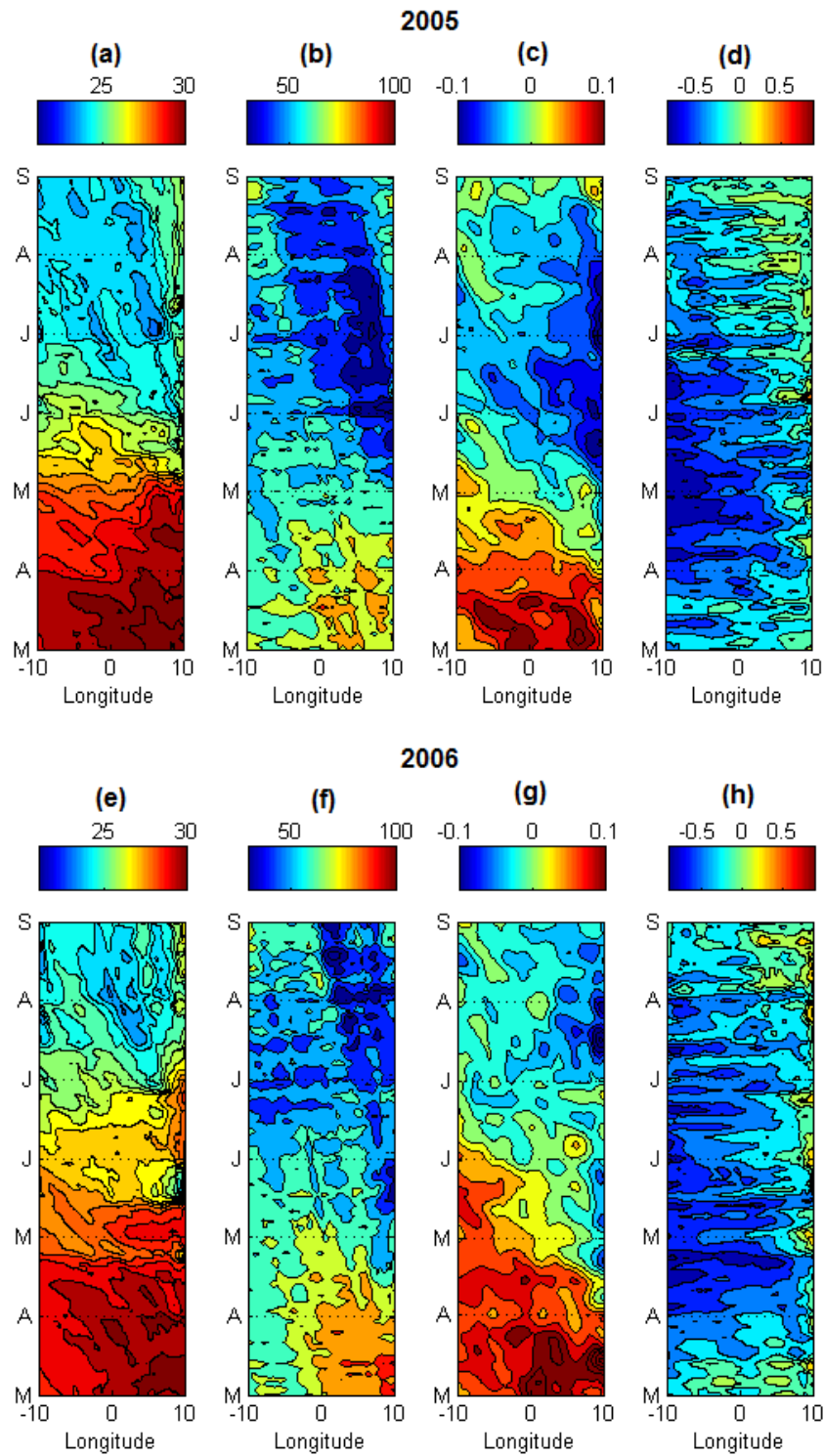
477 In 2005, the locally wind-forced component of the wave might reinforce the remote part of the reflected wave
 478 signal at the coast by the sea level slope which balanced the strengthening of alongshore winds blowing during
 479 the mid-May and late-May events. The quantitative and respective contributions of local and remote wind
 480 forcing to this wave is out of the scope of this study and would require further analysis. This phenomenon is
 481 supported in 2005 by anomalous eastward expanded southerly wind bursts observed in May 2005. The month of

482 May is also a period when westward surface currents are usually maximum (as visible on the mean seasonal
483 cycle shown in Fig.1c). Thus, the combined effects of westward surface currents (via advection and vertical
484 mixing through horizontal current vertical shear), local wind influences (via vertical mixing) and wave
485 westward propagation, resulted in the extension of cold upwelled water from the eastern coast to near 20° W.

486 In 2006, the westward extension of cold waters established later, from the beginning of July. A coastal cooling
487 occurred on 18-26 May but no westward extension of the cold waters is observed at this period (Fig. 9e). In
488 2005, the two upwelling Kelvin waves followed each other closely while in 2006, the first Kelvin upwelling
489 wave reached the coast in May and the second in July (Fig.5b & Fig. 6b and Fig. 9f). In addition, the
490 intraseasonal wind strengthening responsible of the coastal cooling on 18-26 May 2006 is less intense (wind
491 stress mean in the CLR $\sim 0.04\text{N.m}^2$) than the one in mid-May 2005 ($\sim 0.06\text{N.m}^2$); which is preceded and followed
492 by another wind bursts few days before and after; Fig. 3b & Fig. 4b).

493 The analysis over 1998-2008 period shows that the westward extension of the cold SST takes place every year
494 but begins at different times of the year (not shown). It occurs generally from June-July, when the cooling
495 events usually occur in the east at this location, and is thus closely linked with the shoaling of the thermocline
496 due to the arrival of a Kelvin upwelling wave at the eastern coast

497



498

499 **Figure 9:** Time-longitude diagrams at 3° S between 10° W and 10° E, and from 2-days averaged model outputs from 1st
 500 March to 31 August 2005 and 2006, of (a & e) the sea surface temperature (° C); (b & f) the 20° C isotherm-depth (m); (c &
 501 g) the sea level anomalies from AVISO data (m); and (d & h) the zonal component of surface velocity (m.s⁻¹).

502

503 In conclusion to this section 4, the SST variability in the CLR at intraseasonal time scales is the result of
504 combination between basin preconditioning by remotely forced shoaling of the thermocline via Kelvin wave,
505 local mixing induced by current vertical shear, and upwelling processes in response to strong southerly winds.
506 As highlighted for the 26-28 May 2005 and 2 April 2006 events, the net heat flux may also contribute to cool
507 the surface waters, through enhanced cloud cover which decrease the incoming solar radiation. The cold
508 upwelled waters around 3°S extend then westward from the eastern coast to near 20°W by combined effect of
509 the westward propagating Rossby waves as well as vertical mixing and advection processes. The cool water may
510 thus contribute to the cooling in the southern edge of the cold tongue region. Although the processes implied
511 differ slightly due to the presence of the coast, the SST variability in the CLR is quite close to the one in the
512 equatorial cold tongue region (not shown), due to similar atmospheric forcing. However, for a given wind burst,
513 the intensity of SST response in the CLR and in the cold tongue region is modulated by subsurface conditions
514 which are under the influence of equatorial Kelvin wave. In May 2005, the Kelvin wave reached the eastern
515 coast while three wind bursts occurred. The thermocline was thus shallower in the east than west of 0°W,
516 providing favorable subsurface conditions making the coupling between making the SST more reactive to wind
517 intensification occurred during this month. In addition, the decrease short wave radiations due to enhanced cloud
518 cover during the 26-28 May 2005 event or 2 April 2006 event, which contribute to the cooling in the CLR, did
519 not concern the equatorial region east of 0°W.

520

521 **5. Focus on the mid-May 2005 event**

522 We have previously identified five main cold events in 2005 (22-24 April, 8-12 May, 16-20 May, 26-30 May
523 and 14-18 June), characterized by a temperature drop ranging from -0.2° C to -1.7° C in the model. Analysis of
524 intraseasonal wind stress magnitude (Fig. 4b) has revealed that each event is associated with strengthening of
525 equatorward winds, especially during the 14-16 May event when the intraseasonal wind stress magnitude
526 averaged over the CLR is the strongest one. This particular event has been found to be responsible for the
527 sudden and intense SST cooling in the eastern equatorial Atlantic and identified as part of manifestation of
528 temporal variability of the St. Helena Anticyclone (Marin et al., 2009). In this section, we focus on this mid-
529 May event, to better understand the processes at play during this unusual event.

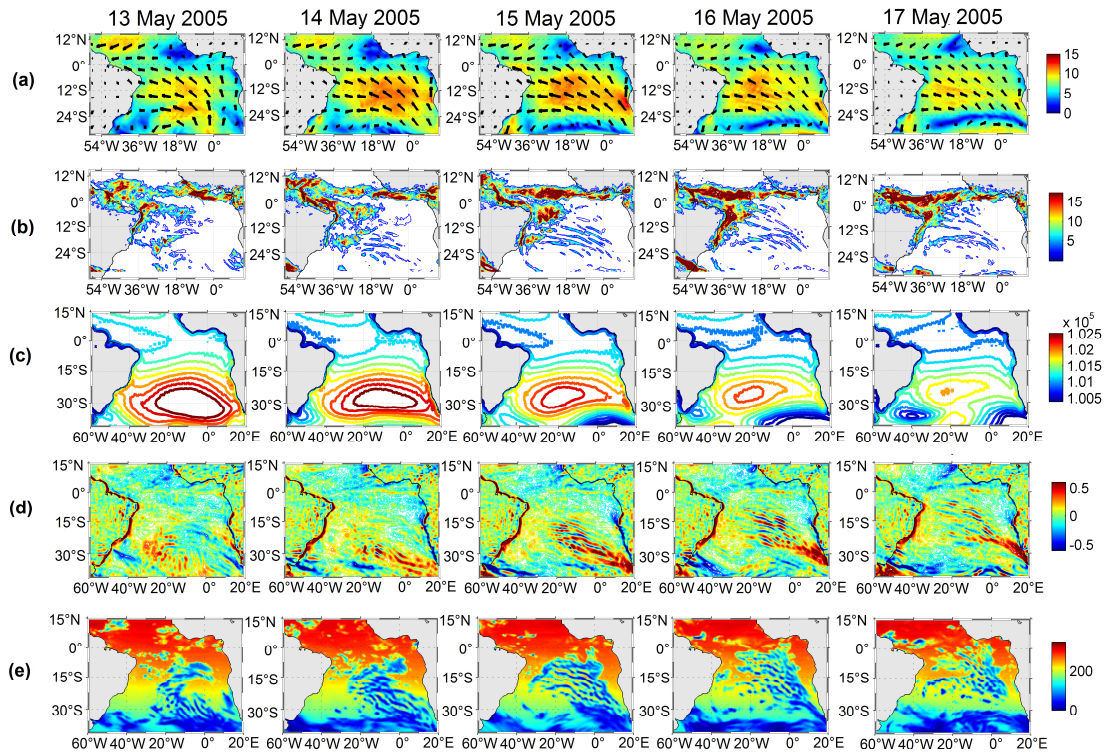
530 **5.1 Atmospheric conditions**

531

532 **5.1.1 Wind and surface atmospheric pressure**

533 The spatial distribution of the mid-May 2005 wind event can be inferred from Fig. 10 where CFSR wind speed
534 fields superimposed with daily precipitation fields, surface pressure, wind speed curl, and downward shortwave
535 radiation, are presented from 13 May to 17 May. The event was characterized by intense southeasterly wind east
536 of 15° W and from 30°S to the equator from 13-14 May, concomitant with a strengthening of the easterlies west
537 of 30° W between 30° and 15° S (Fig. 10a). The strong southeasterly winds drifted then westward up to 15-16
538 May when the maximum was located in the western part of the basin off northeastern Brazilian coast.
539 Simultaneously, a strengthening of southerly winds occurred north of the equator in the Gulf of Guinea. The

540 strong winds during the event were associated with high pressure core of the Saint Helena Anticyclone,
 541 especially on 13-14 May, also associated with particularly low pressure under the ITCZ 4 days later (Fig. 10c).
 542 The pressure fall during the mid-May 2005 event appeared as the lowest in May over the whole decade (not
 543 shown). The meridional surface pressure gradient during the event is thus found to be the strongest over 1998-
 544 2008 period. That suggests strong Hadley circulation intensity during the mid-May event and therefore strong
 545 equatorward moisture flux, allowing the deep atmospheric convection in the Gulf of Guinea to be triggered at a
 546 self-sustaining level (see Sect. 5.2 following).



547

548 **Figure 10:** Daily-averaged, from 13 May to 17 May 2005 (left to right panels), of (a) wind magnitude (color
 549 field) (m.s^{-1}) superimposed with wind vectors from CFSR fields; (b) precipitation rate ($\text{kg.m}^{-2}.\text{day}^{-1}$) from
 550 CFSR fields; (b) surface pressure (hPa) from ERA-20C reanalysis; (c) wind speed curl (m.s^{-1}) computed from
 551 CFSR wind speed fields; and (d) downward short-wave radiation (W.m^{-2}) from CFSR fields.

552 5.1.2 Precipitation

553

554 The maps of precipitation rate during the event (Fig. 10b) display a band of heavy precipitation ($9-17 \text{ kg.m}^{-2}.\text{day}^{-1}$)
 555 between $5^{\circ} - 9^{\circ} \text{ N}$ and off northeast Brazil from the coast to 15° W and from 10° S to 3° S . The
 556 maximum precipitation rate in this region occurred on 15-16 May concomitant with the easterly winds
 557 strengthening. This convective zone, located between the ITCZ north of the equator and the South Atlantic
 558 Convergence Zone (SACZ) in southern tropics, is the Southern Intertropical Convergence Zone (SICZ)
 559 (Grodsky and Carton, 2003). This zone forms usually later, by June-August, when the southern branch of the
 560 convection separates from the ITCZ which moves north of the equator. Grodsky and Carton (2003) showed that

561 this rainfall pattern appears closely linked to the seasonal change in SST difference between the ACT region
562 (which they defined between 15° W – 5° W, 2° S – 2° N) and the SITCZ region (25° W - 20° W, 10° S - 3° S).
563 They argued that the seasonal appearance of the ACT along the equator sets up pressure gradients within the
564 boundary layer that induce wind convergence in the SITCZ region. Based on Grodsky and Carton (2003)
565 results, the unusually rainfall conditions during mid-May event might thus be explained by strong SST gradient
566 between the two regions caused by unusually early cooling in the ACT region at this time of the year.

567

568 **5.1.3 Generation of atmospheric gravity wave**

569

570 The precipitation fields during the mid-May event (Fig. 10b) also evidence rainfall pattern typical of
571 atmospheric gravity wave train characterized by a horizontal wave length ~ 500 km and initiated by a front
572 system (forming the northern boundary of a low pressure system) which developed around 17° S on 14 May and
573 traveled northeastward until 17 May. The rainfall train was associated with oscillatory wind speed curl train
574 alternating between positive and negative values (Fig. 10d) as well as alternating downward shortwave radiation
575 minimum (Fig. 10e) associated with the wave clouds. Gravity waves are known to play an important role in
576 transporting the momentum and energy through long distances (Fritts, 1984). Here, they would be a way to
577 carry momentum and energy from South Atlantic to the equator during the strong event.

578

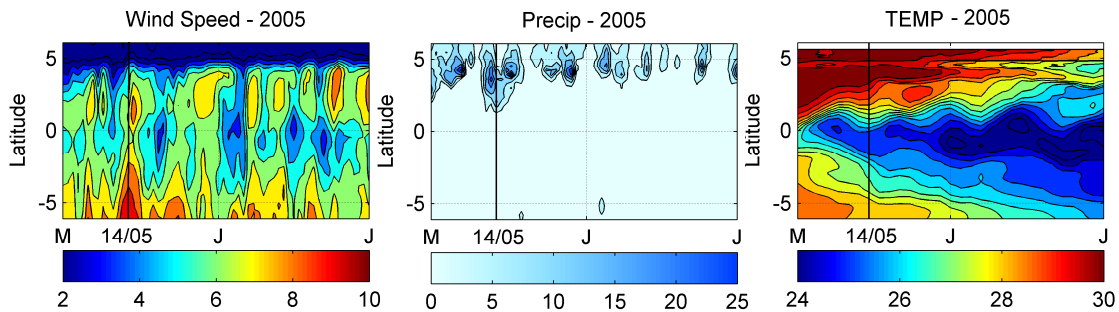
579 **5.2 A decisive event for coastal monsoon onset**

580 The mid-May 2005 wind event was found to be involved in the early onset of the ACT development (Marin et
581 al. 2009, Caniaux et al., 2011). The influence of the cold tongue on the WAM onset has been suggested by
582 several authors (Okumura and Xie, 2004; Caniaux et al., 2011; Nguyen et al., 2011; Thorncroft et al., 2011). At
583 the seasonal time-scale, Caniaux et al. (2011) suggest that it comes from strong interactions between the SST
584 cooling and wind pattern in the eastern equatorial Atlantic: the ACT serves to accelerate (decelerate) winds in
585 the northern (southern) hemisphere contributing to the northward migration of humidity and convection, and
586 pushes precipitation to the continent. Thus, due to its impact on ACT development, the mid-May 2005 wind
587 event is also linked to the onset of the WAM in 2005 which has been the earliest over 1982-2007 period from
588 Caniaux et al. (2011). In this section we aim to better understand how this single wind event may have such
589 impact. For further information on the WAM, the reader can refer to Leduc-Leballeur et al. (2013) and Caniaux
590 et al. (2011).

591

592 In order to analyze the air-sea pattern in the northern Gulf of Guinea during May-June 2005, we show in Fig. 11
593 the wind magnitude, precipitation rate, and SST fields averaged from 10° W to 6° W. The wind strengthening
594 appeared first south of the equator on 12-16 May and then north of the equator from 14-18 May. It was
595 associated with strong rainfall extending southward up to 2° N. Equatorial cooling occurred 4 days after the
596 event and slowed down the overlying winds by feedback mechanisms. The winds north of the equator then
597 remained stronger than in the ACT region and strengthened again north of the Equator on 22-28 May together
598 with precipitation maximum pushed northward (around 5° N) after the event.

599 Thus, this mid-May event appears as the “decisive event” which triggered the abrupt transition between the two
600 wind patterns in the northern Gulf of Guinea, when the wind north of the equator became and remained stronger
601 than south of the equator. It occurred 15 days earlier than the average date (31 May) identified by Leduc-
602 Leballeur et al. (2013) over 2000-2009 period. According to these authors, the time of occurrence of this
603 phenomenon would be related with the strength of anomalous moisture flux. They explain that in April-May the
604 low atmospheric local circulation is present only during an equatorial SST cooling and surface wind
605 strengthening north of the equator, both generated by a southerly wind burst, before disappearing until the next
606 wind burst. In June-July the low atmospheric local circulation is then always present and intensified by the wind
607 bursts. Thus, the establishment of an abrupt seasonal transition event as observed in 2005, occurring much
608 earlier than the reference date, supposed anomalously strong equatorial cooling caused by unusual strong
609 southerly winds which allowed, through air-sea interactions mechanisms, to trigger the deep atmospheric
610 convection in the Gulf of Guinea at a self sustaining level.



611

612 **Figure 11:** Time evolution, in May and June 2005 between 6° S and 6° N and averaged between 10° W and 6°
613 W, of the (a) daily averaged wind magnitude ($\text{m}\cdot\text{s}^{-1}$) from CFSR wind fields ; (b) daily averaged precipitation
614 rate ($\text{kg}\cdot\text{m}^{-2}/\text{day}$) from CFSR fields and (c) 2-daily averaged SST ($^{\circ}\text{C}$) fields, from the forced model.

615

616 5.3. What made the mid-May 2005 event so special?

617

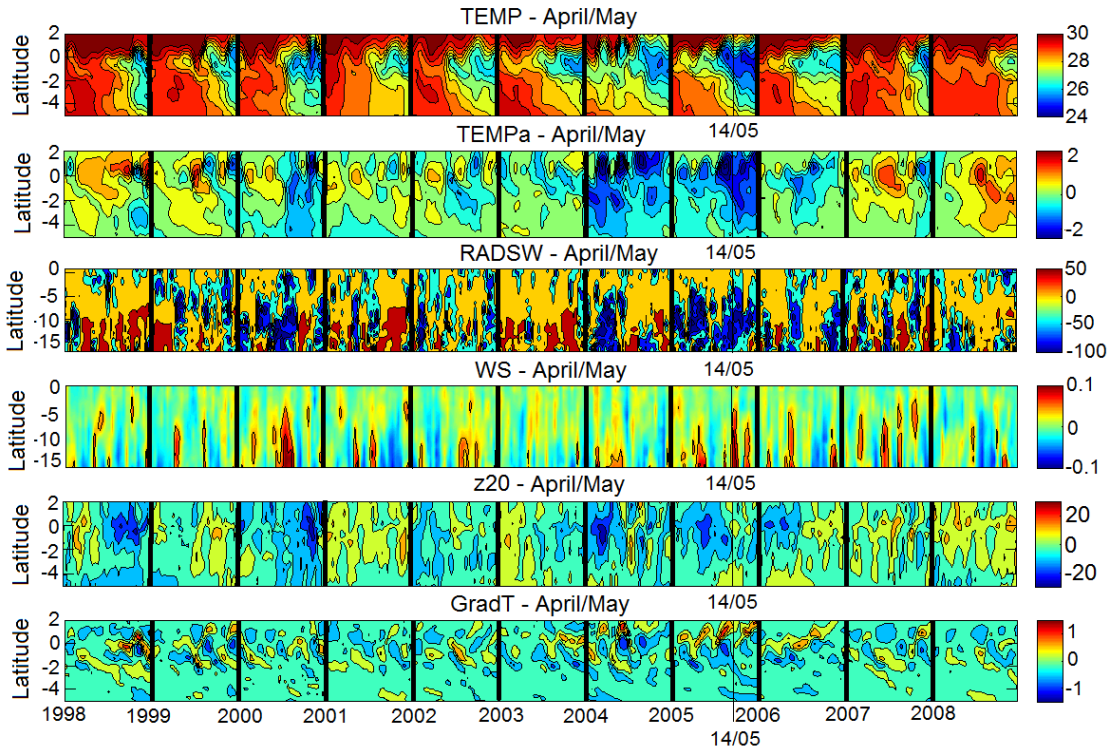
618 To better understand which makes the particularity of the mid-May 2005 event, the atmospheric and oceanic
619 conditions (SST, intraseasonal SST anomalies, intraseasonal short-wave radiation flux anomalies (hereafter
620 RADSW), intraseasonal wind stress magnitude anomalies, intraseasonal z20 anomalies, and intraseasonal
621 meridional SST gradient anomalies) averaged over the 10° W - 6° W region and between 15° S to 5° N during
622 April-May are analyzed over the 1998-2008 period (Fig. 12). The intraseasonal wind stress magnitude anomaly
623 during mid-May event appears to be one of the strongest over the whole 1998-2008 period (up to $0.13\text{N}\cdot\text{m}^{-2}$
624 around 15°S and $0.05\text{N}\cdot\text{m}^{-2}$ in equatorial region). These strong wind conditions are usually met later in late
625 boreal spring or summer, when the St. Helena Anticyclone strengthens and shifts northward toward the warm
626 hemisphere. The wind intensification in mid-May 2005 was associated with particularly weak RADSW from
627 South Atlantic to the northern equatorial region, suggesting cloud albedo effect during the event which tended to
628 cool the mixed layer. We can notice that the April-May 2005 period was characterized by the lowest mean
629 RADSW.

630 In addition, at the time of the event, the surface waters were already cooled by previous wind bursts (e.g. 20
631 April and 8 May). The SST response to the mid-May event occurred 4-6 days later, inducing the weakest
632 equatorial SST values for April-May season over the whole 1998-2008 period (SST drop of $\sim 3^{\circ}\text{C}$ inducing SST
633 $< 24.8^{\circ}\text{C}$). The cooling also caused an enhanced SST front around 1°N , as shown in Fig. 12 (bottom panel),
634 which was found to be the earliest and strongest one over the 1998-2008 period. This meridional SST gradient
635 was responsible for the wind surface intensification north of the equator (Fig. 11a and Fig. 12, fourth panel)
636 through air-sea interaction mechanisms as described by Leduc-Leballeur et al. (2011). Another SST gradient
637 maximum is found at the end of May 1998 but it was not extended as eastward than during the mid-May 2005
638 event (not shown).

639 When the wind burst occurred on 14 May 2005, the 20°C -isotherm depth in the area was anomalously shallow
640 south of the equator and slightly deeper at the equator (Fig. 12, fifth panel). The thermocline shoaling associated
641 with the Kelvin wave appeared in fact a few days earlier providing favorable subsurface conditions which made
642 the SST response to previous wind bursts (20 April and 8 May) more effective. At the time of the mid-May
643 event, the wave already reached more eastern areas, as shown in previous sections.

644
645 Thus, the particularity of the mid-May 2005 event mainly lies in the i) anomalous atmospheric conditions
646 related to strong St. Helena Anticyclone perturbation; ii) cooling initiated by the succession of previous wind
647 bursts; and iii) favorable subsurface local ocean conditions preconditioned by equatorial waves which shoaled
648 the mixed layer. Another wind burst of comparable intensity occurred at the beginning of May 2000 (Fig. 12,
649 fourth panel) while the thermocline was shallow, causing SST cooling at the equator (Fig. 12, first and second
650 panels). However, the wind strengthening was less sudden than during the mid-May 2005 event and the
651 resulting cooling took place over a less broad region (not shown). In addition, the surface pressure drop in the
652 ITCZ region was not as pronounced as during mid-May 2005 event.

653



654

655 **Figure 12:** Time-latitude diagrams for April-May along the 1998-2008 period, of 2-days average, from top to
 656 bottom i) SST ($^{\circ}\text{C}$); ii) intraseasonal anomaly of SST ($^{\circ}\text{C}$); iii) intraseasonal anomaly of short-wave radiation
 657 surface flux (W.m^{-2}) from CFSR fields; iv) intraseasonal anomaly of wind stress magnitude (N.m^{-2}) from CFSR
 658 fields; v) intraseasonal anomaly of 20°C -isotherm depth (m) computed from the forced model SST; vi)
 659 intraseasonal anomaly of meridional SST gradient (every 0.5° of latitude), from the forced model; averaged over
 660 10°W - 6°W . The vertical black thin line indicates the date of 14 May, 2005. For details about the calculations
 661 of the anomalies, see Sect. 2.

662

663 6. Summary and discussion

664 In this study, the impact of intraseasonal winds on SST in the far eastern Tropical Atlantic during boreal spring
 665 2005 and 2006 has been investigated from observations and numerical simulation. We first focus our study in
 666 the Cape-Lopez region (CLR), east of 5°E and between the equator and 7°S , where the seasonal and interannual
 667 SST variability is poorly documented. There, the boreal spring (AMJ) season corresponds to a transitional
 668 period between high SST in boreal winter and low ST in boreal summer, under the influence of local winds.
 669 Intensified cool SSTs are observed in the coastal upwelling area located around 6°S in the Congo mouth region,
 670 associated with mean alongshore wind conditions. Boreal spring season is in fact characterized by maximum
 671 winds amplitude, influence of which is made more effective by shallow thermocline depth, itself strongly
 672 influenced by remote forcing. The seasonal cycle in the CLR is modulated by strong year-to-year variations, as
 673 observed in boreal spring 2005 when cold SST anomaly are associated with shallower-than-average thermocline
 674 depth and positive wind speed anomaly.

675 The intraseasonal wind bursts which occurred in boreal spring 2005 and 2006 generated cooling episodes
676 especially around 3°-4° S except for some strongest events when the cooling reached more northern equatorial
677 region, especially during the mid-May and end-May 2005 events. The intensity of the cold events resulted from
678 basin preconditioning by remotely forced shoaling of the thermocline (via Kelvin wave), local mixing (induced
679 by current vertical shear) and upwelling processes in response to strong southerly local winds. For one particular
680 event, on 26-28 May 2005, the net heat flux also tended to cool the surface water, due to enhanced cloud cover
681 which decreased the incoming solar radiations. In the CLR, stronger wind intensification and favorably
682 preconditioned oceanic subsurface conditions in 2005 made the coupling between surface and subsurface ocean
683 processes more efficient than in 2006, resulting in stronger cooling. It should be noted that the occurrence of
684 intraseasonal wind intensification in the CLR is not specific to the boreal spring/summer 2005 and 2006 and is
685 observed every year over the 1998-2008 period of study (not shown). However, their impact on SST variability
686 in the region is modulated depending of the strength of wind intensification and of the subsurface
687 preconditioning. For example, the year 1998, known as a "warm year", is characterized by anomalous warm
688 SST in boreal spring/summer in the CLR., associated with anomalous weak winds and anomalous deep
689 thermocline.

690 The preconditioning of subsurface conditions in the area via Kelvin wave at the dates of the wind bursts
691 depended on the atmospheric conditions in the western part of the basin a few weeks earlier. Previous studies
692 (e.g. Picaut, 1983; Philander, 1990) suggest that the source of an equatorial Kelvin wave is mainly related to a
693 sudden change of the zonal wind in the west. Analysis of atmospheric and oceanic conditions at intraseasonal to
694 daily scale in winter 2005 and 2006 showed that for both years, an Kelvin upwelling wave was initiated in the
695 west while easterly winds were strengthened from either side of the equator just after the ITCZ to be at its
696 southernmost location. This latter was observed one month earlier in 2006 (late February – early March) than in
697 2005 (late March-early April), and was associated with a negative wind stress curl anomaly. In winter 2005, the
698 ITCZ was found south of the equator after a very sudden southward shift and was followed by strong easterlies
699 during ~20 days. In winter 2006, the ITCZ was found closer to the equator less sharply and during a longer
700 period, followed by weaker easterlies when compared to 2005. These results obtained for the years 2005 and
701 2006 years do not imply that same atmospheric conditions would be observed for winter upwelling Kelvin wave
702 of other years. Especially, the year 2005 was very particular and also exhibited anomalously cold SSTs in the
703 south Atlantic and anomalously warm SSTs in the north Atlantic initiated in fall 2004, signature of a meridional
704 mode (Virmani and Weisberg, 2006; Foltz and McPhaden, 2006; Hormann and Brandt, 2009).

705 Upon impingement at the eastern boundary, the incoming equatorial Kelvin wave excites westward-propagating
706 Rossby waves and poleward propagating coastal Kelvin waves. In 2005, the Kelvin wave reached the coast
707 around mid-May while southerly winds strengthened, allowing the reflected wave to be reinforced by the local
708 wind. This resulted in westward propagation of negative z20 and SSH anomalies which, combined with
709 enhanced westward surface currents, provided favorable conditions to westward extension of cold upwelled
710 water from the eastern coast to near 20°W through advection and vertical mixing.

711

712

713 In the second part of the study, we specially focused on the mid-May 2005 event (13 May to 16 May) that was
714 characterized by strong southerly wind strengthening in the eastern Tropical Atlantic Ocean. It was found to be
715 responsible for the sudden and intense SST cooling in the Gulf of Guinea and the CLR, and involved in the early
716 onset of the ACT development in 2005 and therefore in the early onset of the WAM. The analysis of
717 atmospheric and oceanic conditions in the Gulf of Guinea associated with this event allowed to show that the
718 mid-May event, controlled by the St. Helena Anticyclone, can be identified as a “decisive event” which
719 triggered the abrupt transition between two wind patterns in the northern Gulf of Guinea. Unusual strong
720 southerly winds induced anomalously strong equatorial cooling which in turns slowed down the overlying wind
721 feedback mechanism and generated stronger than normal southerlies north of the equator through the SST front
722 around 1°N. This triggered the deep atmospheric convection in the Gulf of Guinea at a self-sustaining level and
723 the beginning of coastal precipitation. The time of occurrence of this phenomenon, 15 days earlier than the
724 averaged date (31 May from Leduc-Leballeur et al., 2013), suggests that the mid-May 2005 event was
725 associated with anomalous strong moisture flux. The description of atmospheric conditions over the 1998-2008
726 period has shown that the 2005 event was characterized by the strongest surface pressure gradient between the
727 St. Helena high pressures and the low pressures under the ITCZ, inducing strong Hadley cell activity. No similar
728 atmospheric pattern was observed during the whole 1998-2008 period. Another wind burst of comparable wind
729 intensity occurred at the beginning of May 2000. This event also induced a cooling at the equator but the surface
730 pressure decrease in ITCZ region was not as pronounced as during mid-May 2005 event and the SST gradient
731 around 1° N was weaker. In addition to coastal precipitation in the Gulf of Guinea and due to the early cooling
732 in the ACT region, unusually rainfall conditions also occurred between the northeast coast of Brazil and 15° W
733 within the SITCZ, which generally forms in early boreal summer.

734 Finally, this study highlights the importance of a strong southerly wind burst in the eastern tropical Atlantic
735 during boreal spring season, which is a transitional period during which an anomalous strong energy input may
736 tip the energy balance from an equilibrium state toward another one and thus impact the WAM system. The
737 analysis of atmospheric and oceanic conditions during the mid-May 2005 wind event allows to highlight the
738 different processes through which the wind power provided by the wind burst is brought to the ocean: i) direct
739 effect of the wind on the SST in the eastern tropical Atlantic; ii) changes in the trade winds in the western
740 equatorial Atlantic exciting eastward-propagating equatorial Kelvin waves; iii) energy transport via
741 atmospheric gravity waves from South Atlantic; and iv) energy supply to Rossby wave. In addition to unusual
742 atmospheric conditions in mid-May 2005, the ocean response intensity to this event was also enhanced by the
743 subsurface conditions, made favorable by previous wind bursts, either local (e.g. in 6-8 May) or occurring a few
744 weeks before in the West.

745 It is crucial to better describe the atmospheric and oceanic processes at play during such extreme event, notably
746 in order to reduce the well known warm bias in the southeastern tropics in coupled models in both atmospheric
747 and oceanic components (Zeng et al., 1996; Davey et al., 2002; Deser et al., 2006; Chang et al., 2007; Richter
748 and Xie, 2008) as well as in forced ocean-only simulations (e.g. Large and Danabasoglu, 2006). This warm bias
749 is well evidenced in our numerical simulation (Fig. 1&2) and our results clearly show that the cooling episodes
750 were underestimated in the CLR, implying the need to investigate more in depth the oceanic and atmospheric
751 processes at play in this particular region. As the intraseasonal wind bursts are related to the fluctuations of St.

752 Helena Anticyclone, their impact on SST variability in the eastern tropical Atlantic and regional climate
753 suggests the need of better understand the St. Helena Anticyclone variability.

754 It is also important to note that the mid-May 2005 event occurred during an unusually active year. The year
755 2005 exhibited a pronounced meridional mode pattern with strong SST gradient between the two hemispheres.
756 Several authors (Foltz et al., 2006 ; Virmani and Weisberg, 2006 ; Marengo et al., 2008a, 2008b ; Zeng et al.,
757 2008) studied this particular year, marked by anomalously warm SST in the tropical North Atlantic during
758 March-July, the warmest from at least 150 years. This anomalous warming was associated with the most active
759 and destructive hurricane season on record (Foltz et al., 2006; Virmani and Weisberg, 2006) and an extreme and
760 rare drought in the Amazon Basin (Marengo et al., 2008a, 2008b; Zeng et al. 2008; Erfanian et al., 2017). From
761 these authors, primary causes of the anomalous warming in 2005 were a weakening of the northeasterly trade
762 winds and associated decrease in wind-induced latent heat loss as well as changes in shortwave radiation and
763 horizontal oceanic heat advection. This 2005 temperature record is made even more remarkable given that,
764 unlike the 1998's one, it occurred in the absence of any strong El Niño anomaly (Shein, 2006). Some studies
765 ([Goldenberg et al., 2001](#)) attribute these SST increases to the Atlantic Multidecadal Oscillation (AMO), while
766 others suggest that climate change may instead be playing the dominant role ([Emanuel, 2005](#); [Webster et al.,
767 2005](#); [Mann and Emanuel, 2006](#); [Trenberth and Shea, 2006](#)). Comparable anomalously warm tropical Atlantic
768 SSTs have been observed in 2010 also associated with extreme drought in the Amazon. However, from time
769 series of monthly anomalies constructed for the two basins (North and South Atlantic) by using OISST monthly
770 mean data, Erfanian et al. (2017) show that the warmer-than-usual SSTs in the North Atlantic in 2010 was not
771 associated with colder-than-usual SST in South Atlantic contrarily to 2005 (their Fig. S4e).

772 While the warming in North Tropical Atlantic during 2005 has been investigated by several authors, the cooling
773 in South Atlantic has received less attention. This study highlights the need to further document and monitor the
774 South Atlantic region and the St. Helena Anticyclone, through additional high resolution analysis and
775 observations.

776

777 Acknowledgments:

778 The research leading to these results received funding from the EU FP7/2007-2013 under grant agreement no.
779 603521, PREFACE and from the EU Horizon 2020 under grand agreement no. 2014-633211, AtlantOS. These
780 projects are gratefully acknowledged. We do thank Gildas Cambon ([IRD/LOPS](#)) for his help and participation
781 on the implementation of ROMS simulations, and Frédéric Marin ([IRD/LEGOS](#)) for his helpful comments. **We
782 would also like to thank NASA, CNES and ECMWF for freely providing data and products used in this study.**

783

784

785 **References:**

786

787 Adamec, D., O'Brien, J. J.: The seasonal upwelling in the Gulf of Guinea due to remote forcing, *J. Phys.*

788 *Oceanogr.*, 8, 1050-1060, 1978.

789
790 Battisti, DS.: Dynamics and thermodynamics of a warming event in a coupled tropical atmosphere ocean model,
791 J. Atmos. Sci. 45:2889 – 2919, 1988.
792
793 Busalacchi, A., Picaut, J.: Seasonal variability from a model of the tropical Atlantic Ocean, J. Phys Oceanogr.,
794 13, 1564-1588, 1983.
795
796 Bourlès, B., Brandt, P., Caniaux, G., Dengler, M., Gouriou, Y., Key, E., Lumpkin, R., Marin, F., Molinari, R.L.,
797 Schmid, C. : African Monsoon Multidisciplinary Analysis (AMMA): Special measurements in the
798 Tropical Atlantic, CLIVAR Exchange Letters, 41 (12 2), International CLIVAR Project Office,
799 National Oceanography Centre, Southampton, United Kingdom, 7–9, 2007.
800
801 Brandt, P., Funk, A., Hormann, V., Dengler, M., Greatbatch, R.J., Toole, J.M.: Interannual atmospheric
802 variability forced by the deep equatorial Atlantic Ocean, Nature, 473, 497–500,
803 doi:10.1038/nature10013, 2011.
804
805 Caniaux, G., Giordani, H., Redelsperger, J.-L., Guichard, F., Key, E., Wade, M.: Coupling between the Atlantic
806 cold tongue and the West African monsoon in boreal spring and summer, J. Geophys. Res., 116,
807 C04003, doi:10.1029/2010JC006570, 2011.
808
809 Carton, J. A., Chepurin, G., Cao, X., Giese, B.S.: A simple ocean data assimilation analysis of the global upper
810 ocean 1950 –1995, part 1: Methodology, J. Phys. Oceanogr., 30, 294–309, doi:10.1175/ 1520-
811 0485(2000)030<0294:ASODAA>2.0.CO;2, 2000a.
812
813 Carton, J. A., Chepurin, G., Cao, X.: A simple ocean data assimilation analysis of the global upper ocean 1950–
814 1995, part 2: Results, J. Phys. Oceanogr., 30,311–326, doi:10.1175/1520-0485(2000)
815 030<0311:ASODAA>2.0.CO;2, 2000b.
816
817 Carton, J. A., and Giese, B.S.: A reanalysis of ocean climate using simple ocean data assimilation (SODA),
818 Mon. Weather Rev., 136 ,2999–3017, doi:10.1175/2007MWR1978.1, 2008.
819
820 Colin, C.: Sur la variabilité dans le Golfe de Guinée: Nouvelles considérations sur les mécanismes d’upwelling,
821 Ph.D. thesis, Mus. Natl. d’Hist. Nat., Paris, 1989.
822
823 Chang, C.-Y., Carton, J.A., Grodsky, S.A., Nigam, S.: Seasonal climate of the tropical Atlantic sector in the
824 NCAR Community Climate System Model 3: Error structure and probable causes of errors, J. Climate,
825 20, 1053–1070, 2007.
826
827 Chelton, D. B., deSzoeko, R.A., Schlax, M. G. , Naggar, K. E., Siwertz, N.: Geographical variability of the first-
828 baroclinic Rossby radius of deformation, J. Phys. Oceanogr., 28, 433–460, 1998.

829
830 Dai, A., and Trenberth, K.E.: Estimates of freshwater discharge from continents: Latitudinal and seasonal
831 variations, *J. Hydrometeorol.*, 3, 660–687, 2002.
832
833 Danabasoglu, G., Large, W.G., Tribbia, J.J., Gent, P.R., Briegleb, B.P.: Diurnal Coupling in the Tropical
834 Oceans of CCSM3, *Journal of Climate*, 19, 2347-2365, 2006.
835
836 Davey, M., Huddleston, M., Sperber, K.R., et al.: STOIC: A study of coupled model climatology and variability
837 in tropical ocean regions, *Clim. Dynam.*, 18, 403-420, 2002.
838
839 [Debreu, L., Marchesiello, P., Penven, P., Cambon, G.](#): Two-way nesting in split-explicit ocean models:
840 algorithms, implementation and validation, *Ocean Modelling*, 49-50, 1-21, 2012.
841
842 De Coëtlogon, G., Janicot, S., Lazar, A.: Intraseasonal variability of the ocean-atmosphere coupling in the Gulf
843 of Guinea during boreal spring and summer, *Q. J. R. Meteorol. Soc.*, 136, 426–441, doi:10.1002/qj.554,
844 2010.
845
846 Denamiel, C., Budgell, W.P., Toumi, R.: The Congo River plume: Impact of the forcing on the far-field and
847 near-field dynamics, *J. Geophys. Res. Oceans*, 118, 964–989, doi:10.1002/jgrc.20062, 2013.
848
849 Deser, C., Capotondi, A., Saravanan, R., Phillips, A.: Tropical Pacific and Atlantic climate variability in
850 CCSM3, *J. Climate*, 19, 2451–2481, 2006.
851
852 Djakouré, S., Penven, P., Bourlès, B., Veitch, J., Koné, V.: Coastally trapped eddies in the north of the Gulf of
853 Guinea, *J. Geophys. Res. Oceans*, 119, 6805–6819, doi:10.1002/2014JC010243, 2014.
854
855 Emanuel, K.: Increasing destructiveness of tropical cyclones over the past 30 years, *Nature*, 436, 686-688, 2005.
856
857 Erfanian, A., Wang, G., Fomenko, L.: Unprecedented drought over tropical South America in 2016:
858 significantly under-predicted by tropical SST, *Scientific reports*, 7:5811, doi: 10.1038/s41598-
859 017_05373-2, 2017.
860
861 [European Centre for Medium-Range Weather Forecasts: ERA-20C Project \(ECMWF Atmospheric Reanalysis](#)
862 [of the 20th Century\). Research Data Archive at the National Center for Atmospheric Research,](#)
863 [Computational and Information Systems Laboratory, Boulder, CO. \[Available online at](#)
864 <https://doi.org/10.5065/D6VQ30QG>], 2014. Accessed 25 Jan 2017.
865
866 Foltz, G. R., Grodsky, S. A., Carton, J. A., McPhaden, M. J.: Seasonal mixed layer heat budget of the tropical
867 Atlantic Ocean, *J. Geophys. Res.*, 108, 3146, doi:10.1029/2002JC001584, 2003.
868

869 Foltz, G.R. and McPhaden, M.J.: Unusually warm sea surface temperatures in the tropical North Atlantic during
870 2005, *Geophys. Res. Lett.*, 33: doi: 10.1029/2006GL027394. issn: 0094-8276, 2006.
871

872 Fritts, D. C.: Wave saturation in the middle atmosphere: A review of theory and observations, *Rev. Geophys.*,
873 22, 275–308, 1984.
874

875 Gentemann, C.L., Wentz, F.J., Brewer, M., et al.: Passive Microwave Remote Sensing of the Ocean: an
876 Overview, *Oceanography from Space, Revisited*, edited by V. Barale, J. Gower, and L. Alberotanza,
877 13–33. Heidelberg: Springer, 2010.
878

879 Giese, B.J, Harrison, D.E.: Aspects of the Kelvin wave response to episodic wind forcing, *J. Geophys. Res.*, 95:
880 7289 – 7312, 1990.
881

882 Giordani, H., Caniaux, G., Voldoire, A.: Intraseasonal mixed-layer heat budget in the equatorial Atlantic during
883 the cold tongue development in 2006, *J. Geophys. Res.: Oceans*, 118(2):650-671. doi:
884 10.1029/2012JC008280, 2013.
885

886 Goldenberg, S.B., Landsea, C.W., Mestas-Nuñez, A.M., Gray, W.M.: The Recent Increase in Atlantic Hurricane
887 Activity: Causes and Implications, *Science*, 293, 474-479, doi: 10.1126/science.1060040, 2001.
888

889 Grodsky, S. A., Carton, J. A.: The Intertropical Convergence Zone in the South Atlantic and the Equatorial Cold
890 Tongue, *J. Climate*, 16, 723–733, 2003.
891

892 Haidvogel, D.B., Beckmann, A.: *Numerical Ocean Circulation Modeling*, Imperial College Press, London; 320
893 pp., 1999.
894

895 Herbert, G., Boulès, B., Penven, P., Grelet, J.: New insights on the upper layer circulation north of the Gulf of
896 Guinea, *J. Geophys. Res.: Oceans*, 121, doi:10.1002/2016JC011959, 2016.
897

898 Hormann, V., Brandt, P.: Upper equatorial Atlantic variability during 2002 and 2005 associated with equatorial
899 Kelvin waves, *J. Geophys. Res.*, 114: C03007, doi:10.1029/2008JC005101, 2009.
900

901 Illig, S., Dewitte, B., Ayoub, N., du Penhoat, Y., Reverdin, G., Mey, P.D., Bonjean, F., Lagerloef, G.S.E.:
902 Interannual long equatorial waves in the tropical Atlantic from a high-resolution ocean general
903 circulation model experiment in 1981-2000, *J. Geophys. Res.: Oceans*, 109:C02022. doi: 10.1029/
904 2003JC001771, 2004.
905

906 Jouanno, J., Marin, F., duPenhoat, Y., Sheinbaum, J., Molines, J.M.: Seasonal heat balance in the upper 100m of
907 the Equatorial Atlantic Ocean, *J. Geophys. Res.: Oceans*, 116:C09003. doi: 10.1029/2010JC006912,
908 2011.

909
910 Jouanno, J., Marin, F., duPenhoat, Y., Molines, J.M.: Intraseasonal Modulation of the Surface Cooling in the
911 Gulf of Guinea, *J. Phys. Oceanogr.*, 43(2):382-401. doi: 10.1175/JPO-D-12-053.1, 2013.
912
913 Krishnamurti, T. N., Pasch, R.J., Ardanuy, P.: Prediction of African waves and specification of squall lines,
914 *Tellus*, 32, 215-231, 1980.
915
916 Leduc-Leballeur, M., Eymard, L., de Coëtlogon, G.: Observation of the marine atmospheric boundary layer in
917 the Gulf of Guinea during the 2006 boreal spring, *Q. J. R. Meteorol. Soc.*, 137: 992 – 1003, 2011.
918
919 Leduc-Leballeur, M., de Coëtlogon, G., Eymard, L.: Air – sea interaction in the Gulf of Guinea at intraseasonal
920 time-scales: Wind bursts and coastal precipitation in boreal spring, *Q. J. R. Meteorol. Soc.*, 139, 387–
921 400, doi:10.1002/qj.1981, 2013.
922
923 Lübbecke, J.F., Burls, N.J., Reason, C.J.C., McPhaden, M.J.: Variability in the South Atlantic Anticyclone and
924 the Atlantic Nino Mode, *J. Climate*, 27, doi: 10.1175/JCLI-D-14-00202.1, 2014.
925
926 Mann, M. E., and Emanuel, K.A.: Atlantic hurricane trends linked to climate change, *Eos, Trans. Amer.*
927 *Geophys. Union*, 87, 233–244, 2006.
928
929 Marengo, J. A., Nobre, C.A., Tomasella, J., Oyama, M.D., De Oliveira, G.S., De Oliveira, R., Camargo, H.,
930 Alves, L.M., Brown, I.F. : The drought of Amazonia in 2005, *J. Climate*, 21, 495-516, 2008a.
931
932 Marengo, J.A., Nobre, C.A., Tomasella, J., Cardoso, M.F., Oyama, M.D.: Hydro-climatic and ecological
933 behaviour of the drought of amazonia in 2005, *Philosophical transactions of the Royal society of*
934 *London, Biological sciences*, v.21, p.1-6, 2008b.
935
936 Marin, F., Caniaux, G., Bourlès, B., Giordani, H., Gouriou, Y., Key, E.: Why were sea surface temperatures so
937 different in the Eastern Equatorial Atlantic in June 2005 and 2006, *J. Phys. Oceanogr.*, 39, 1416–1431,
938 doi:10.1175/2008JPO4030.1, 2009.
939
940 Materia, S., Gualdi, S., Navarra, A., Terray, L.: The effect of Congo River freshwater discharge on Eastern
941 Equatorial Atlantic climate variability, *Clim. Dynam.*, 39(9-10), 2109–2125, doi:10.1007/s00382-012-
942 1514-x, 2012.
943
944 McCreary, J.: Eastern tropical ocean response to changing wind systems with application to El Nino, *J. Phys.*
945 *Oceanogr.*, 6, 632-645, 1976.
946
947 McCreary, J., Picaut, J., Moore, D.: Effects of the remote annual forcing in the eastern tropical Atlantic Ocean,
948 *J. Mar. Res.*, 42, 45 81, 1984.

949 Merle, J. : Conditions hydrologiques saisonnières de la marge continentale du Gabon et du Congo (de 10°N a
950 60°S) Etude descriptive, Dot. Sci. O.R.S.T.O.M. Pointe-Noire, 27 : 1-20, 1972.
951

952 Merle, J., Fieux, M., Hisard, P.: Annual signal and interannual anomalies of sea surface temperature in the
953 eastern equatorial Atlantic Ocean, *Deep Sea Res.*, 26,77–101, 1980.
954

955 Mitchell, T. P., Wallace, J.M.: The annual cycle in equatorial convection and sea surface temperature, *J.*
956 *Climate*, 5, 1140–1156, 1992.
957

958 Moore, D.W.: Planetary-gravity waves in an equatorial ocean, PhD Thesis, Harvard University, 201 pp., 1968.
959

960 Moore, D.W., and Philander, S.G.H.: Modeling of the tropical ocean circulation, *The Sea*, Vol. 6, Wiley
961 Interscience, New York, N.Y., pp. 316-361, 1977.
962

963 Moore, D. W., Hisard, P., McCreary, J. P., Merle, J., O'Brien, J. J., Picaut, J., Verstraete, J. M., Wunsch, C.:
964 Equatorial adjustment in the eastern Atlantic, *Geophys. Res. Lett.*, 5, 637-640, 1978.
965

966 Nguyen, H., Thorncroft, C. D., Zhang, C.: Guinean coastal rainfall of the West African Monsoon, *Q.J.R.*
967 *Meteorol. Soc.*, 137: 1828–1840. doi:10.1002/qj.867, 2011.
968

968 Nicholson, S.E., Dezfuli, A.K.: The relationship of rainfall variability in western equatorial Africa to the tropical
969 oceans and atmospheric circulation. Part I: The boreal spring, *J. Climate*, 26(1), 45–65, 2013.

970

970 Nobre, P., Shukla, J.: Variations of sea surface temperature, wind stress, and rainfall over the tropical Atlantic
971 and South America, *J. Climate*, 9 : 2464 – 2479, 1996.
972

973 Okumura, Y., and Xie, S.P.: Interaction of the Atlantic equatorial cold tongue and the African monsoon, *J.*
974 *Climate*, 17, 3589–3602, 2004.
975

976 Okumura, Y., Xie, S.P.: Some overlooked features of tropical Atlantic climate leading to a new Niño-like
977 phenomenon, *J. Climate*, 19(22), 5859–5874, doi:10.1175/JCLI3928.1, 2006.
978

979 Ostrowski, M., Da Silva, J. C. B., Bazik-Sangolay, B.: The response of sound scatterers to El-Niño and La Niña-
980 like oceanographic regimes in the southeastern Atlantic, *ICES J. Mar. Sci.*, 66 (6), 1063-1072, doi:
981 10.1093/icesjms/fsp102, 2009.
982

983 Penven, P., Marchesiello, P., Debreu, L., Lefevre, J.: Software tools for pre- and post-processing of oceanic
984 regional simulations, *Environ. Modell. Software*, 23, 2008 660–662, 2008.
985

986 Peter, A.-C., Le Hénaff, M., du Penhoat, Y., Menkès, C., Marin, F., Vialard, J., Caniaux, G., Lazar, A.: A model
987 study of the seasonal mixed layer heat budget in the equatorial Atlantic, *J. Geophys. Res.*, 111, C06014,
988 doi: 10.1029/2005JC003157, 2006.

989
990 Philander, S., and Pacanowski, R.: A model of the seasonal cycle in the Tropical Atlantic Ocean, *J. Geophys.*
991 *Res.*, 91, 14, 192–14, 206, 1986.
992
993 Philander, S.G.: *El Nino, La Nina and the Southern Oscillation*, Academic Press, 293 pp., 1990.
994
995 Picaut, J.: Propagation of the seasonal upwelling in the eastern equatorial Atlantic, *J. Phys. Oceanogr.*, 13, 18–
996 37, doi: 10.1175/1520-0485, 1983.
997
998 Picaut, J.: On the dynamics of the thermal variations in the Gulf of Guinea, *Oceanogr. Trop.*, 19 (2) : 127-53,
999 1984.
1000
1001 Piton, B. : Les courants sur le plateau continental devant Pointe-Noire (Congo), Documents scientifiques,
1002 ORSTOM, Brest, n°47, 37 p., 1988.

1003 Polo, I., Lazar, A., Rodriguez-Fonseca, B., Arnault, S.: Oceanic Kelvin waves and tropical Atlantic
1004 intraseasonal variability: 1. Kelvin wave characterization, *J. Geophys. Res.*, 113, C07009, doi: 10.1029/
1005 2007JC004495, 2008.
1006
1007 Redelsperger, J. L., et al. : AMMA: Une étude multidisciplinaire de la mousson Ouest-Africaine, *Meteorologie*,
1008 54,22–32, doi:10.4267/2042/20098, 2006.
1009
1010 Richter, I. and Xie, S.-P.: On the origin of equatorial Atlantic biases in coupled general circulation models,
1011 *Clim. Dynam.*, 1:587–598, doi : 10.1007/s00382-008-0364-z, 2008.

1012 Rouault, M., Servain, J., Reason, C. J. R. , Bourlès, B., Rouault, M. J. , Fauchereau, N.: Extension of PIRATA
1013 in the tropical south-east Atlantic: An initial one-year experiment, *Afr. J. Mar. Sci.*,31(1),63–71,
1014 doi:10.2989/AJMS.2009.31.1.5.776, 2009.
1015
1016 Saha, S., Moorthi, S., Pan, H.-L., Wu, W., Wang, J., Nadiga, S., Tripp, P., Kistler, R., Woollen, J., Behringer,
1017 D., Liu, H., Stokes, D., Grumbine, R., Gayno, G., Wang, J., Hou, Y.T., Chuang, H.-Y., Juang, H.-M.
1018 H., Sela, J., Iredell, M., Treadon, R., Kleist, D., Van Delst, P., Keyser, D., Derber, J., Ek, M., Meng, J.,
1019 Wei, H., Yang, R., Lord, S., Van Den Dool, H., Kumar, A., Wang, W., Long, C., Chelliah, M., Xue, Y.,
1020 Huang, B., Schemm, J.-K., Ebisuzaki, W., Lin, R., Xie, P., Chen, M., Zhou, S., Higgins, W., Zou, C.-Z.
1021 Z., Liu, Q., Chen, Y., Han, Y., Cucurull, L., Reynolds, R.W., Rutledge, G., Goldberg, M. : The NCEP
1022 climate forecast system reanalysis, *Amer. Meteor. Soc.*, 91, 1015-1057, 2010.
1023
1024 Schouten, M. W., Matano, R. P., Strub, T. P.: A description of the seasonal cycle of the equatorial Atlantic from
1025 altimeter data, *Deep-Sea Res.*, Part I, 52, 477–493, doi:10.1016/j.dsr.2004.10.007, 2005.
1026

1027 Servain, J., Picaut, J., Merle, J.: Evidence of remote forcing in the equatorial Atlantic Ocean, *J. Phys. Oceanogr.*,
1028 12, 457–463, 1982.
1029

1030 Shein, K. A.: State of the climate in 2005, *Bull. Am. Meteorol. Soc.*, 87, s1–s102, doi: 10.1175/BAMS-87-6-
1031 shein, 2006.
1032

1033 Shchepetkin, A., McWilliams, J.C.: The Regional Oceanic Modeling System (ROMS): A split-explicit, free-
1034 surface, topography-following-coordinate ocean model, *Ocean Modell.* 9, 347–404, 2005.
1035

1036 Thorncroft, C. D., Nguyen, H., Zhang, C., Peyrillé, P.: Annual cycle of the West African monsoon: regional
1037 circulations and associated water vapour transport, *Q. J. R. Meteorol. Soc.*, 137, 129-147,
1038 doi:10.1002/qj.728, 2011.
1039

1040 Trenberth, K.E., Shea, D.J.: Atlantic hurricanes and natural variability in 2005, *Geophys. Res. Lett.*, vol. 33,
1041 L12704, doi: 10.1029/2006GL026894, 2006.
1042

1043 Virmani, J. I., and Weisberg, R.H.: The 2005 hurricane season: An echo of the past or a harbinger of the future?.,
1044 *Geophys. Res. Lett.*, 33, L05707, doi: [10.1029/2005GL025517](https://doi.org/10.1029/2005GL025517), 2006.
1045

1046 Wade, M., Caniaux, G., du Penhoat, Y.: Variability of the mixed layer heat budget in the eastern equatorial
1047 Atlantic during 2005–2007 as inferred using Argo floats, *J. Geophys. Res.*, 116, C08006, doi:
1048 10.1029/2010JC006683, 2011.
1049

1050 Yu, L., Jin, X., Weller, R.A.: Role of net surface heat flux in seasonal variations of sea surface temperature in
1051 the tropical Atlantic ocean, *J. Climate*, 19, 6153–6169, 2006.
1052

1053 Waliser, D. E., and Gautier, C.: A satellite-derived climatology of the ITCZ, *J. Climate*, 6, 2162–2174, 1993.
1054

1055 Wauthy, B. : Introduction à la climatologie du Golfe de Guinée, *Oceanogr. Trop.*, 18, 103–138, 1983.
1056

1057 Webster, P.J., Holland, G. J., Curry, A., Chang, H.R.: Changes in tropical cyclone number, duration, and
1058 intensity, in warming environment, *Science*, 309, 1844-1846, 2005.
1059

1060 Wentz, F.J., and Meissner, T.: Algorithm Theoretical Basis Document (ATBD), version 2, AMSR-E Ocean
1061 Algorithm, Remote Sensing Systems Tech. Rep., RSS 121599A-1, 55 pp., 2000.
1062

1063 White, R.H. and Toumi, R.: River Flow and Ocean Temperatures: The Congo River, *J. Geophys. Res. -Oceans*,
1064 119, 25016–2517, doi:10.1002/2014JC009836, 2014.
1065

1066 Zebiak, S.: Air-sea interaction in the equatorial Atlantic region, *J. Climate*, 6(8), 1567–1586, doi:10.1175/1520-
1067 0442(1993)006<1567:AIITEA>2.0.CO;2, 1993.
1068
1069 Zeng, N., Dickinson, R.E., Zeng, X.: Climatic impact of Amazon deforestation-A mechanistic model study, *J.*
1070 *Climate*, 9, 859–883, 1996.
1071
1072 Zeng, N., Dickinson, R.E., Zeng, X.: Causes and impacts of the 2005 Amazon drought, *Env. Res. Lett.*, 3, doi:
1073 10.1088/1748-9326/3/1/014002, 2008.
1074